I.O.S.

SWANSEA BAY (SKER) PROJECT
TOPIC REPORT: 5

A.D. HEATHERSHAW, A.P. CARR AND H.L. KING

WAVE DATA: OBSERVED AND COMPUTED WAVE CLIMATES

REPORT NO 99
1980

NATURAL ENVIRONMENT RESEARCH COUNCIL
INSTITUTE OF OCEANOGRAPHIC SCIENCES

INSTITUTE OF OCEANOGRAPHIC SCIENCES

Wormley, Godalming,
Surrey, GU8 5UB.
(0428 - 79 - 4141)

(Director: Dr. A.S. Laughton)

Bidston Observatory,
Birkenhead,
Merseyside, L43 7RA.
(051 - 653 - 8633)

(Assistant Director: Dr. D.E. Cartwright)

Crossway,
Taunton,
Somerset, TA1 2DW.
(0823 - 86211)

(Assistant Director: M.J. Tucker)

SWANSEA BAY (SKER) PROJECT

TOPIC REPORT:5

A D HEATHERSHAW, A P CARR AND H L KING

Wave data: Observed and computed wave climates

REPORT NO 99

1980

This project was supported financially by the Department of the Environment

Institute of Oceanographic Sciences
Crossway
Taunton
Somerset

CONTENTS

LIST OF TABLES

LIST OF FIGURES

LIST OF APPENDICES

SUMMARY

This report is the fifth in the Topic Report series concerning Swansea Bay.

Wave data have been used to determine the wave climate of the area and to investigate alongshore variations in wave energy and their relation to the equilibrium of the beach on the E side of the Bay.

Evidence is presented which indicates that over the central portion of the Bay, the alignment of the coastline is locally adjusted to the directions of wave approach in such a way as to minimise longshore movements of sediment (littoral drift). Most of the wave energy goes into producing 'up-beach' or 'down-beach' movements of sediment. This behaviour suggests that the Bay, as a whole, is in equilibrium with the prevailing wave climate, although a net fall in beach level has occurred in the vicinity of Sker Point. The latter may be brought about by increasing obliquity of wave approach at the coast as a result of wave energy focussing behind offshore banks. When considered in relation to the tidal dynamics of the area (see Topic Report 4, Heathershaw and Hammond, 1979b) such behaviour could result in a transfer of sediment from the beach to the offshore banks (Scarweather Sands, Hugo Bank and Kenfig Patches). Long term adjustments of the coastline in the vicinity of Sker Point may also have resulted in the observed southerly movement of the Scarweather Sands (see Topic Report 1, Carr and Blackley, 1977).

1. INTRODUCTION

Coastal erosion processes are, in general, a balance between those effects due to tidal currents and those due to wave action. This balance is simply a function of the geographical location of a particular site and its exposure to the prevailing wave climate and tidal streams.

Since in general tidal currents become weaker at the coast and consequently wave energy becomes a relatively more important factor on our shores, it does not seem unreasonable to assume that wave climate has been responsible for the fashioning of much of our present day coastline.

This report describes the wave climate at a specific site, Swansea Bay on the S Wales coast, UK, (Figure 1), and in particular the way in which beach processes on the foreshore to the S of Port Talbot (see Figure 2) are related to the wave climate.

Sediment transport processes due to tidal and wave induced currents in the offshore and foreshore areas have been described elsewhere (see Heathershaw and Hammond, 1979a and Wilkinson, 1980).

2. WAVE CLIMATE

At any site the spectrum of surface gravity waves is likely to be made up of components due to locally generated seas and those due to longer period swell waves refracting into the area. Since swell waves may originate well outside the area of interest, and be generated under wind conditions which are atypical for the area, it is important to distinguish between these two components in the following discussion.

2.1 Fetch and duration characteristics

The range of wave heights present in a locally generated sea will be a function of the wind speed, fetch and duration. If either fetch or duration are limited then the sea will not reach a fully developed state. Clearly at a site in a coastal embayment, the range of fetch directions will be narrower than that on a more open coastline. Furthermore, it is not sufficient to consider the geometric fetch alone (ie distance that wind blows over the sea surface) as being a true measure of the wind's effectiveness in generating a sea. This is because the wind transfers energy to the sea over a range of angles up to 45° on either side of the direction in which it is blowing and thus open ocean fetches are a measure of the wave energy arriving at a point from a similar range of angles 45° on either side of the wind. In effect this assumes a fetch of infinite

width whereas on an irregular coastline, or in estuaries, rivers and lakes, the fetch width may limit contributions from the full range of angles. Under these conditions wave height prediction is normally carried out in terms of an effective fetch which, usually, is less than the geometric fetch.

For Swansea Bay we have calculated the effective fetch characteristics at Port Talbot using the method given by the Coastal Engineering Research Center (CERC, 1973) and outlined in Appendix A. Effective and geometric fetch characteristics are shown in Table 1 and Figure 3. Figure 3 illustrates that the peaked geometric fetch characteristics are smoothed when considered in terms of effective fetch, and the open ocean fetch, of the order of 6500km, dominates the fetch characteristics for the Bay.

The effective fetch characteristics (see Table 1) have been used to predict wave heights at Port Talbot using the method given by Darbyshire and Draper (1963) (see Figure 4). Tables 2 and 3 show that for wind speeds of 10 and 20ms^{-1} and for durations of 6, 12 and 24 hours, fetch limited conditions occur over a considerably smaller range of angles than would be deduced from the geometric fetches alone. For typical wind speeds (Table 2) significant wave heights (H_s) of the order of 2m are predicted and during storms (Table 3) H_s is predicted to be of the order of 5.5m.

It is interesting to note that during a period of particularly severe storms in November 1977, observed wave heights (H_s) at Port Talbot were about 4.6m with local wind speeds of the order of 20m s^{-1}.

2.2 Wave measurements

During the period December 1975 - December 1977, wave measurements were carried out in the Swansea Bay area at the locations shown in Figure 2. Table 4 lists the data available for the two sites.

At the Scarweather light vessel, measurements were made with a Waverider buoy and at Port Talbot a cabled-in sea bed FM pressure wave recorder was used. The analysis and preliminary interpretation of data from these instruments is described elsewhere (Fortnum and Hardcastle, 1979 a, b).

Wave direction characteristics were also recorded at Port Talbot using an X-band radar (see Heathershaw et al, 1980), and these results are discussed later.

Waverider and sea bed pressure wave recorder data were recorded using frequency modulation on magnetic tape. The recordings were of 1350 seconds duration at the Waverider buoy and 675 seconds for the sea bed recorder. In both

cases records were taken at intervals of 3 hours. These were replayed to give significant wave height H_s (from mean rectified wave height) and the mean zero crossing period T_z. It should be mentioned that due to the attenuation of pressure variation with depth, the pressure recorders respond less to short period waves than the Waverider buoy. To reduce this discrepancy, appropriate correction factors were calculated from an empirical attenuation formula (Draper, 1957), using the actual depth and measured T_z.

The seasonal variations in significant wave height (H_s) at both sites are summarised in Figure 5. This shows a substantial increase in wave heights at the Scarweather Light vessel over those at Port Talbot, and the usual seasonal trend of increased wave heights during the winter months. During the winter months the mean wave heights offshore are of the order 1.8 to 2.2m whereas at Port Talbot they attain a maximum mean value of 1.4m. The seasonal trend is further illustrated in Figures 6, 7, 8 and 9, which show a shift to higher and longer period waves at both sites during the winter months from 6 to about 10s, and the annual summaries of wave period data in Figure 10, which show that a wave period of 8s is fairly typical of the area as a whole.

3. WAVE REFRACTION

In this study wave refraction analyses have been carried out to elucidate the following points:

(a) the possibility of wave energy focussing by offshore banks;
(b) the alongshore variations in wave energy;
(c) the relationship between the direction of wave approach and shoreline equilibria and littoral drift processes.

In the following section a brief review of the salient features of wave refraction theory is given to familiarise the reader with the underlying physical processes. This description is based upon that given in Goldsmith et al (1974).

3.1 General principles

The process whereby waves are slowed, shortened and steepened as they travel into progressively shallower water is called shoaling. Typically this will not occur uniformly along a wave front and as the wave speed (or celerity) decreases in accordance with its shortest wavelength, the wave front bends as a result of the variations in celerity along the front. The combination of shoaling and wave front bending is known as refraction.

The celerity c of a progressive surface water wave is given by linear wave theory as

$$c^2 = \frac{gL}{2\pi} \cdot \tanh \frac{2\pi h}{L} \qquad (1)$$

where g is the acceleration due to gravity, L is the wavelength and is the water depth.

Rearrangement of equation (1), with $c = L/T$ where T is the wave period, gives

$$L = \frac{gT^2}{2\pi} \cdot \tanh \frac{2\pi h}{L} \; . \qquad (2)$$

For deep water $\tanh 2\pi h/L \rightarrow 1$ and so the wavelength L is a function of wave period only. The deep water assumption is valid to within 0.5% for depths greater than one-half of the wavelength.

The effects of shoaling and refraction can be estimated by linear wave theory. For example, the propagation of surface waves into shallow water may be analysed by consideration of the wave energy between vertical planes which are orthogonal to the wave crests and which intersect with the surface to produce wave rays. Energy is assumed to be transmitted between these planes, that is it does not travel along wave crests or cross wave rays. If it is further assumed that the wave period is constant and that there is no net gain or loss of energy by reflection, percolation or bottom friction, then linear wave theory provides the result,

$$\frac{H}{H_0} = K_r K_s \qquad (3)$$

where H_0 is the deep water wave height, H is the inshore wave height and K_r and K_s are the refraction and shoaling coefficients respectively, given by,

$$K_r = \left(\frac{b_0}{b}\right)^{1/2} \qquad (4)$$

and

$$K_s = \left(\frac{2}{2kh + \sinh 2kh}\right)^{1/2} \cdot \qquad (5)$$

Here, b_o and b are the deep water and shallow water wave ray separations respectively (see Figure 11).

As a surface wave travels into shallower water the sea bottom exerts an influence on it, because of the effect of depth in determining the wave celerity (equation 1). When the crests of a train of waves are not parallel to the bottom contours (lines of constant depth) the section in shallow water decreases in speed in such a way that the wave crests tend to become parallel to the bathymetry. Wave refraction diagrams are used to illustrate the way in which a wave of a given period responds to the bottom topography and are constructed in accordance with the principles outlined previously, using Snell's law to determine the direction and celerity along a wave ray. Consequently it is assumed that

$$\frac{\sin \alpha_2}{\sin \alpha_1} = \frac{c_2}{c_1}, \qquad (6)$$

which by optical analogy gives the angles of incidence α_1 and α_2 and the speeds c_1 and c_2 of a wave ray passing from one refractive medium into another, in this case at two different depths.

One of the major difficulties with wave refraction analyses has been due to crossed rays, or caustics, where the energy conservation principles outlined previously indicate infinite amounts of energy as the ray separation $b \to 0$. However this is not now thought to be the problem that it once was (see Goldsmith, 1974) since wave rays have been found to emerge from caustic regions on the continued ray path, the wave conditions being determined by the wave ray separation more or less as if the caustic had not been there. However, there should be a phase shift which according to Goldsmith is not observable due to the randomness of the waves in nature.

Wave refraction diagrams, incorporating the above principles, have been used extensively in this study to elucidate features of the wave climate in Swansea Bay. Such calculations, based on linear wave theory, can be used to predict inshore wave climates from the corresponding measured or predicted offshore climate (eg Abernethy and Gilbert, 1974). However, the calculations make certain assumptions so that they are practicable in terms of run-time and cost. For example:

(a) the seabed topography is approximated by a mesh of finite size which excludes the small scale features;

(b) the energy losses through breaking waves and bottom and surface stress are neglected.

3.2 Methods

The wave refraction calculations described here were carried out using methods developed by the Hydraulics Research Station (HRS, 1974). Details of the theory behind the computations are given in Appendix B.

In particular these computer based techniques have been used for:

(a) ray tracking (see Appendix B1) and

(b) energy calculations (see Appendix B2).

The energy calculations are done in three stages:

(a) Firstly, the sea bed topography information is used to determine energy transfer functions for the directional wave spectrum $S(f,\theta)$ at inshore target points where wave height (or energy) estimates are required. Here f is the wave frequency and θ the direction of wave propagation.

Starting at a target point ray paths are tracked outwards, in a seaward direction, for a discrete set of equally spaced frequencies. The rays are started at equally spaced angular increments suitable for the frequency. HRS found that it was possible to use larger increments for the upper end of their frequency band than for the lower (see HRS, 1974). The rays halt at 'obstacles' or on the grid boundary. Since the paths are reversible, only the rays which reach the deep-water boundary are of interest, but their exact position is immaterial since the spectrum is assumed constant along the deep water boundary.

Longuet-Higgins (1957) has shown that $c\,c_g\,S(f,\theta)$ is constant along a ray path. Here c is the wave celerity and c_g is its group speed. Thus it is possible to calculate transfer functions which give the inshore frequency spectrum from an offshore directional spectrum.

(b) An offshore('deep-water') directional spectrum can be determined from measured wave data either by assuming some form of distribution for both frequency and direction, or the frequency distribution form may be replaced by a frequency spectrum obtained directly from the wave data.

A modified Pierson-Moskowitz spectrum (HRS, 1974, and Pierson and Moskowitz, 1964) was used to approximate the frequency spectrum in this study. The relation between this spectrum and those which were actually observed is discussed later.

The offshore spectral matrix is obtained by evaluating the directional spectrum at each frequency and angular segment. These segments are distinct from the angular increments mentioned in (a) and may be several orders of magnitude larger. The segment size is chosen so that $S(f,\theta)$ is approximately independent of θ in each segment.

(c) The inshore predictions of significant wave height and mean zero crossing period can be calculated from the inshore frequency spectrum for each target point (see later).

For the energy transfer function calculations the sea bed topography was described by depth values taken from Admiralty Charts. The bathymetry was digitised on a grid having overall dimensions of 25 x 25km and made up of 50 x 50 elements having dimensions .5 x .5km. The size and orientation of the grid was chosen to include the offshore banks (ie White Oyster Ledge, Scarweather Sands, Hugo Bank and Kenfig Patches, see Figure 2), to minimise the land area, and to make the x axis roughly coincident with the expected direction of wave approach (see Figure 12). For comparisons of observed and predicted wave heights (see section 3.3), an offshore angular segment size was taken as 15°. In the case of the longshore energy calculations (see section 3.4) an angular segment of 20° was used. In both cases a discrete frequency band width of .05 to .25 Hz was used although the intervals, .01 Hz and .02 Hz respectively, were different. The choice of angular ray separation, inshore, was that used by HRS (1974), namely $\frac{1}{2}^{\circ}$ for 0.05 to 0.15Hz and $\frac{3}{4}^{\circ}$ for 0.17 to 0.25Hz. The functions were calculated for each water level above chart datum that corresponded with the water depths associated with the observed wave parameters.

3.3 Ray tracking

The area covered by the wave refraction analysis is shown in Figure 12. Ray tracking was carried out for a range of water depths, wave periods and offshore wave directions. These are summarised in Table 5. To account for the large tidal range in the area (mean spring range at Swansea of 8.6m) wave refraction analyses were carried out for wave periods of 6, 8 and 10s and for water depths equivalent to chart datum (CD) + 1.00m, CD + 5.25m and CD + 9.50m.

To investigate the different directional characteristics a range of offshore wave directions were investigated in 10° intervals from 220° to 250° (Table 5). This corresponded to a range of wave directions from the SW sector. (For energy

calculations this directional span was extended to encompass the range 220° to 270°, but only for waves where T_z = 8s, and a height of 1m; see 3.4 below). In addition a range of wave directions from the SE sector was investigated corresponding to directions of 150° to 170° in 10° intervals. Examples of the ray tracking work are shown in Figures 13 - 14 with further examples given in Appendix C. All bearings are in degrees from True North.

The ray tracking diagrams show clearly the effect of wave energy focussing by the offshore banks, particularly the Scarweather Sands, for the range of wave periods and water depths examined. For directions of wave approach in the SW sector focussing leads to increasing obliquity of wave approach at the coast as one moves from Port Talbot towards Sker Point (Figures 2 and 13).

3.4 Observed and predicted wave heights

As a precursor to the longshore energy calculations described in the following sections comparisons of predicted and observed wave heights at Port Talbot were undertaken using the wave refraction model. In an earlier study by IOS in Start Bay, Devon, preliminary validations of the wave refraction calculations were carried out (King and Hardcastle, 1980). This work provided one of the few reported comparisons between inshore wave climates predicted from wave refraction calculations and those obtained from actual measurements. As in Start Bay, the Swansea Bay offshore wave climate, in terms of significant wave height and zero crossing period, was required in order to predict the inshore values of H_s and T_z prior to comparing the latter with observed values. The H_s and T_z values used in the present analysis were those obtained from the Waverider buoy located near the Scarweather light vessel (Figure 2) while the offshore direction was estimated from the angle of wave approach at Port Talbot as determined by radar and from the directions of the prevailing winds (see Figure 2 and Heathershaw et al, 1980).

The data so obtained produced a total of 41 comparable observations of both H_s and T_z from the inshore and offshore wave recorders. These data corresponded to:

(a) a water depth above chart datum of 5.25 $\pm$ .5m (roughly mean sea level), and
(b) offshore wave approach directions in the range 220-260°.

The results of these comparisons are illustrated in Figures 15 and 16.

The predicted inshore values of H_s were calculated using the Pierson-

Moskowitz spectrum (see Appendix B3) parameterized in terms of the corresponding offshore H_s and T_z values. Figure 15 shows that as the direction of wave approach is increased from 220° to 260° there is closer agreement between observed and predicted values although there is still a tendency for predicted H_s values to over-estimate observed values by some 10 - 20%. Offshore wave approach directions greater than 260° are bounded by the S Gower coastline (Figure 2 and Table 1). Figure 16 shows observed and predicted values of T_z which are characteristically more scattered with no discernable improvement in correlation as the wave approach direction is increased from 220° to 260°.

Differences between theoretical and actual forms of offshore wave spectra may lead to differences between observed and predicted inshore wave climates. The comparisons of H_s shown in Figure 15 are between those values obtained from the Pierson-Moskowitz (PM) spectrum (Appendix B.3) and those values obtained directly from the wave record (see Fortnum and Hardcastle, 1979 a, b for details of H_s and T_z calculations). Figures 17 and 18 show that the PM form may depart significantly from the actual spectrum of the waves calculated from a Fast Fourier Transform (FFT) of their record. An alternative procedure of calculating the PM spectrum from H_s and T_z values obtained from the FFT spectrum, tends to under-estimate the peak energies in the actual (FFT) wave spectrum. Comparisons of observed and predicted H_s values calculated in these 3 ways are given in Figure 19 which shows that the actual (FFT) spectrum provides better agreement than the PM spectrum calculated from H_s and T_z values obtained directly from the wave record. It is also interesting to note that, despite underestimating the peak energies the PM spectrum calculated from the FFT H_s and T_z values also gives good agreement (Figure 19b).

Despite these differences and principally for computational ease we have used the Pierson-Moskowitz (PM) spectrum for the wave energy and beach variability calculations which follow.

3.5 Energy calculations

3.5.1 Method. As noted above energy calculations were carried out for offshore wave directions between 220° and 270° at 10° intervals. These were restricted to a wave period (T_z) of 8 seconds, which is representative for the area, and a wave height (H_s) of 1m. For Port Talbot the annual mean wave height (H_s) is 0.5m with 21.5% of waves exceeding 1m but only 3.9% exceeding 2m. Wave energy coefficients, E, (see below) were calculated for each of 3 water levels (1.0, 5.25, and 9.5m above Chart Datum) at each of the

11 sites where beach profiles had been surveyed monthly between September/October 1975 and April/May 1977. In order to maximise the number of rays reaching the shoreline some slight adjustment of the target points was made for sections E, V, X and Z, (Figure 2).

A Pierson-Moskowitz spectrum was used to define the offshore boundary conditions. The wave energy coefficient (E) used is approximately $(H_s)^2$, the discrepancy, of the order of +2%, being attributable to the use of the particular spectrum in the computations.

The angle of wave incidence for each offshore direction and water level was compared with the measured beach alignment for each line of section. This was calculated from the latest Ordnance Survey 1 : 10,000 or 1 : 10,560 sheets, supplemented, where applicable, by IOS photogrammetry (Blackley and Carr, 1977). Only the low water mark could be determined satisfactorily and even here some difficulties arose. These stem from accuracy of physical measurement; representativeness of conditions at time of topographic survey; and the variability of beach alignment between any pair of beach sections.

Also the computed shoreline wave energy coefficients for each water level and offshore wave direction were compared with the range of height variability, for the 11 beach profiles, over the duration of the surveys.

3.5.2 Results. Wave Incidence and Beach Alignment. Table 6 compares the difference between the beach alignment and the computed wave incidence at the shoreline for water levels of 1.0, 5.25 and 9.5m above CD. Because, irrespective of offshore wave direction, there is very little difference in wave incidence for any specific water level at any survey position, the 6 offshore directions (220° - 270°) have been consolidated to give a mean computed wave incidence and standard deviation. These are then compared with the measured beach alignment. The data are plotted in a simplified fashion in Figure 20. It is clear that apart from the 2 most southerly beach sections, 'X' and 'Z', there is very close agreement between computed and observed angles.

Correlation coefficients have been calculated for the relationship of beach orientation and wave incidence (Table 6) at low, mid and high water levels. For this purpose the beach has been considered as extending from C to T, C to V, C to X or C to Z. Although the significance level always remains better than .001, it is noteworthy that the correlation coefficient falls as 'X' and 'Z' are introduced into the linear regression. The regression also demonstrates that, not unreasonably, the correlations are marginally better between low water mark

and low water level, than between low water mark and other water elevations.

Figure 21 shows the deviation from normal incidence for the various survey lines. In general, such deviation between beach alignment and computed wave incidence is in the same sense for any beach zone but there are minor variations at 'E', 'P' and 'V' with a somewhat greater one at 'T'. Section X is notable for the relatively small discrepancy at low water level but considerably greater ones for mid and high water levels although the direction remains the same.

3.5.3 Wave Energy and Beach Variability. Tables 7 and 8 list the wave energy coefficients (E) for the 1.0, 5.25 and 9.5m above CD water levels for each beach section. Table 7 gives these data for offshore wave directions of 250°, 260° and 270°, while Table 8 gives the same information for directions of 220°, 230° and 240°. Both data sets are also normalised with respect to the mean wave energy (E_L) from the range 250° - 270° at Section L (approximately Port Talbot). The information is represented diagrammatically in Figure 22. It is clear that, apart from Section N, the differences between the wave energy coefficients from 220° - 240° and 250° - 270°, are very largely restricted to the 3 northerly sections, C, E and G. The large standard deviation at 'P' can be attributed to the offshore bathymetry in that area.

Table 9 lists the maximum range of vertical variation along the 11 beach sections over the 18-month survey period during which monthly measurements were carried out. The data are divided up into lower beach change (ie below zero to +3m OD, which is approximately mean sea level); upper beach change (taken from zero fo +3m OD, the latter being approximately the lower limit of the shingle storm beach), and the average for each section as a whole. Figures 23 and 24 show a number of comparisons between beach variability and computed wave energy coefficient. In all cases 'V', 'X' and 'Z' plot away from the rest of the data in a zone marked by relatively low wave energy but high beach variability. It will be recalled that the deviation between the direction of wave incidence and beach alignment is greatest at X and, particularly, Z. Elsewhere, where wave incidence and beach alignment are closely coincident, two contrasting situations occur. For offshore approach directions of 220° and 230° no correlations are found between wave energy and beach variability and this is virtually true for 240° also. In contrast, there are very good correlations between waves from offshore directions of 250°, 260° and 270° (Table 7). Examples of both situations are shown in Figure 24 and Figure 22, respectively. It is interesting to note that although we are only concerned here with relative energy levels, an offshore wave approach direction of 260° gives best agreement between the observed

and predicted wave climates at Port Talbot (section 3.4 and Figure 15c).

There is an excellent case, therefore, for proposing a close and meaningful relationship between wave energy and beach height changes over that section of the shoreline where longshore transport and net volume changes are minimal. Only at Section V, which may be regarded as transitional, is there a poor relationship between beach height range, which is large, and wave energy, which is small, in spite of the close agreement between observed beach alignment and computed wave incidence. Blackley and Carr (1977) point out that since the ending of sand and gravel extraction on the beaches south of Port Talbot tidal harbour in 1973, only beach section Z has shown continuing losses of material. This was equal to 29cm overall between September 1975 and October 1977. Deviation between beach alignment and computed wave incidence reaches a maximum of 25.5° (at mid-water level) here. Thus it would appear that there is a prima facie case for suggesting that although wave energy is relatively low in the southern sections increasing obliquity leads to wave-generated longshore transport. This trend is complemented by increasing tidal currents and residuals towards the south offshore (Heathershaw and Hammond, 1979b) as well as an enhanced drainage network down beach at low water.

4. CONCLUSIONS

Calculation of the fetch characteristics (Figure 3) at Port Talbot confirms that the wave climate in Swansea Bay is dominated to a large extent by its open fetch to the N Atlantic. Tables 2 and 3 show that due to the angular spreading of wave energy the range of fetch limited directions is comparatively small and that locally generated seas arriving from anywhere in the south west sector are limited by the duration of the wind.

Ray tracking (Figures 13 and 14 and Appendix C) has shown that the offshore banks, in particular the Scarweather Sands, but also the White Oyster Ledge, are capable of bringing about wave energy focussing. For waves in the SW sector these effects are particularly pronounced in the region of Sker Point (Figure 2) leading to departures from normal wave incidence at the coast.

This result suggests an alongshore variation in wave energy which might be related to littoral drift and beach variability. This has been confirmed by energy calculations (Figures 23 and 24) which despite some differences between observed and predicted wave climates, show:

(a) where the direction of wave approach at the coast is normal, there is a

significant correlation between wave energy and beach height variability, ie the more energy the greater the variability;

(b) where the direction of wave approach at the coast is not normal, more energy goes into producing a littoral drift, which may lead to net losses of sand from the beach.

5. ACKNOWLEDGEMENTS

This work was supported financially by the Department of the Environment. We are grateful to our colleagues at IOS Taunton for assistance in the preparation of bathymetry and the analysis of wave data.

REFERENCES

ABERNETHY, C.L. and GILBERT, G., 1974. Refraction of a wave spectrum. Hydraulics Research Station Report, INT 117, 87 pp.

BLACKLEY, M.W.L. and CARR, A.P., 1977. Swansea Bay (Sker) Project Topic Report: 2. Evidence for Beach Stability: Photogrammetric and Topographic Measurements. Institute of Oceanographic Sciences Report, No.51, 45 pp.

CARR, A.P. and BLACKLEY, M.W.L. 1977. Swansea Bay (Sker) Project Topic Report: 1(a) Introduction. (b) Long term changes in the coastline. Institute of Oceanographic Sciences Report, No. 42, 63 pp.

CARTWRIGHT, D.E. and LONGUET-HIGGINS, M.S. 1956. The statistical distribution of the maxima of a random function. Proceedings of the Royal Society, A, 231, 212-232.

COASTAL ENGINEERING RESEARCH CENTER (CERC), 1973. Shore Protection Manual Volume 1, 180 pp.

DARBYSHIRE, M. and DRAPER, L. 1963. Forecasting wind-generated sea-waves. Engineering, 195, 482-484.

DRAPER, L. 1957. Attenuation of sea waves with depth. La Houille Blanche, 12, 926-931.

FORTNUM, B.C.H. and HARDCASTLE, P.J. 1979a. Waves recorded at Port Talbot on the South Wales Coast. Institute of Oceanographic Sciences Report, No.78, 8 pp.

FORTNUM, B.C.H. and HARDCASTLE, P.J. 1979b. Waves recorded at Scarweather Bank in the Bristol Channel. Institute of Oceanographic Sciences Report, No.79, 7 pp.

GOLDSMITH, V., MORRIS, W.D., BYRNE, R.J. and WHITLOCK, C.H., 1974. Wave climate model of the mid-Atlantic shelf and shoreline (Virginian Sea). National Aeronautics and Space Administration Special Publication, SP - 358, 146 pp.

HASSELMANN, K. et al. 1973. Measurements of wind growth and swell decay during the Joint North Sea Wave Project (JONSWAP). Deutches Hydrographisches Institut Erganzunscheft Reihe A(8), No.12, 95 pp.

HEATHERSHAW, A.D. and HAMMOND, F.D.C., 1979a. Swansea Bay (Sker) Project Topic Report: 6. Offshore Sediment Movement and its Relation to observed Tidal Current and Wave Data. Institute of Oceanographic Sciences Report, No.93, 119 pp.

HEATHERSHAW, A.D. and HAMMOND, F.D.C., 1979b. Swansea Bay (Sker) Project Topic Report: 4. Tidal currents: Observed tidal and residual circulations and their response to meteorological conditions. Institute of Oceanographic Sciences Report, No.92, 154 pp.

HEATHERSHAW, A.D., BLACKLEY, M.W.L. and HARDCASTLE, P.J. 1980. Wave direction estimates in coastal waters using radar. Coastal Engineering, 3, 249 - 267.

HYDRAULICS RESEARCH STATION (HRS), 1974. Maplin investigations: a wave refraction study in the Thames estuary. Hydraulics Research Station Report, Ex.659, 29 pp.

KING, H.L. and HARDCASTLE, P.J., 1980. Personal communication.

LONGUET-HIGGINS, M.S. 1957. On the transformation of a continuous spectrum by refraction. Proceedings of the Cambridge Philosophical Society, 53, 226-229.

PIERSON, W.J. and MOSKOWITZ, L. 1964. A proposed spectral form for fully developed seas based on the Similarity Theory of S.H.Kitaignodskii. Journal of Geophysical Research, 65, 5181 - 5190.

TABLE 1

Geometric and effective fetches from Port Talbot

Bearing from Port Talbot (^{o}T)	Geometric fetch (km)	Effective fetch (km)
150	45.0	21.0
160	42.2	26.0
170	38.6	30.9
180	38.3	501.9
190	39.0	1102.0
200	42.5	1334.8
210	48.0	2577.0
220	6500.0	2904.2
230	6500.0	3676.4
240	6500.0	3779.7
250	6500.0	3670.3
260	6500.0	3361.0
270	12.5	2560.8
280	12.3	2560.2
290	11.0	1077.8
300	7.5	477.4
310	7.1	7.0
320	6.3	5.7
330	6.0	4.5
340	5.9	3.3

Note: 350^{o} to 140^{o} is range of angles occluded by land.

TABLE 2

Predicted wave heights (H_s) at Port Talbot for a 10m s^{-1} wind blowing for 6, 12 and 24 hours.

Bearing from Port Talbot (^oT)	Effective fetch (km)	Wave height H_s(m) Duration (6 hrs)	(12hrs)	(24hrs)
150	21.2	[.60	[.60	[.60
160	26.0	.65	.65	.65
170	30.9	.70]	.70]	.70]
180	501.9	1.40	1.80	1.90
190	1102.0	1.40	1.80	1.90
200	1334.3	1.40	1.80	1.90
210	2577.0	1.40	1.80	1.90
220	2904.2	1.40	1.80	1.90
230	3676.4	1.40	1.80	1.90
240	3779.7	1.40	1.80	1.90
250	3670.3	1.40	1.80	1.90
260	3361.0	1.40	1.80	1.90
270	2560.8	1.40	1.80	1.90
280	2560.2	1.40	1.80	1.90
290	1077.8	1.40	1.80	1.90
300	477.4	1.40	1.80	1.90
310	7.0	[.25	[.25	[.25
320	5.7	.22	.22	.22
330	4.5	.20	.20	.20
340	3.3	.19]	.19]	.19]

Notes: (a) values of H_s bracketed are fetch limited

(b) values of H_s calculated from Figure 4 after Darbyshire and Draper, 1963.

TABLE 3

Predicted wave heights (H_s) at Port Talbot for a 20m s^{-1} wind blowing for 6, 12 and 24 hours.

Bearing from Port Talbot (^oT)	Effective fetch (km)	Wave height H_s(m) Duration (6 hrs)	(12 hrs)	(24 hrs)
150	21.2	[1.50	[1.50	[1.50
160	26.0	1.70	1.70	1.70
170	30.9	1.80]	1.80]	1.80]
180	501.9	4.70	5.20	5.40
190	1102.0	4.70	5.20	5.50
200	1334.8	4.70	5.20	5.50
210	2577.0	4.70	5.20	5.50
220	2904.2	4.70	5.20	5.50
230	3676.4	4.70	5.20	5.50
240	3779.7	4.70	5.20	5.50
250	3670.3	4.70	5.20	5.50
260	3361.0	4.70	5.20	5.50
270	2560.8	4.70	5.20	5.50
280	2560.2	4.70	5.20	5.50
290	1077.8	4.70	5.20	5.50
300	477.4	4.70	5.20	5.30
310	7.0	[.75	[.75	[.75
320	5.7	.65	.65	.65
330	4.5	.60	.60	.60
340	3.3	.55]	.55]	.55]

Notes: (a) values of H_s bracketed are fetch limited
(b) values of H_s calculated from Figure 4 after Darbyshire and Draper, 1963
(c) during the storm surge of 11 November 1977 the observed significant wave heights at Port Talbot reached a value of about 4.6m with peak local wind speeds of 20m s^{-1}.

TABLE 4

MIAS REF. NO. 443 — ONE DEGREE SQUARE 1402 13

LOCATION
- Position: 51°27′ N 003°55′ W
- Period covered: Start date: 30 Jul 1974 End date: 31 Dec 1977
- Location: Scarweather Bank (Mumbles), Swansea Bay, Bristol Channel.
- Mean water depth: 27 m
- Mean tidal range: 9.0 m (Spring) 4.2 m (Neap)
- Maximum currents: m/sec.

DATA CONTACT
- Organisation: Marine Information and Advisory Service,
- Address: Institute of Oceanographic Sciences, Wormley, Godalming, Surrey GU8 5UB, U.K.
- Report title: Waves Recorded at Scarweather Bank in the Bristol Channel. IOS Report No 79, 1979.

INSTRUMENT
- Instrument type: Waverider
- Type of mounting: Moored to sea bed
- Record duration: 10 min.
- Record interval: 3 hr.

REASON FOR RECORDING: Data gathered for the Swansea Bay (Sker) project financed by the Department of Environment. *

FORM AND MEDIUM OF DATA
- Original data: Frequency modulated magnetic tape.
- Processed data: Listings of Tucker-Draper statistics as printout or on digital magnetic tape.
- Analysed data: Most standard analysis presentations.

NOTES

Data collected by:
Institute of Oceanographic Sciences, U.K.

* Reports available.

MIAS REF. NO. 442 — ONE DEGREE SQUARE 1402 13

LOCATION
- Position: 51°34′ N 003°48′ W
- Period covered: Start date: 16 May 1975 End date: 30 Nov 1977
- Location: Port Talbot, Bristol Channel.
- Mean water depth: 12 m
- Mean tidal range: 8.6 m (Spring) 4.0 m (Neap)
- Maximum currents: m/sec.

DATA CONTACT
- Organisation: Marine Information and Advisory Service,
- Address: Institute of Oceanographic Sciences, Wormley, Godalming, Surrey GU8 5UB, U.K.
- Report title: Waves Recorded at Port Talbot on the South Wales Coast. IOS Report No 78, 1979.

INSTRUMENT
- Instrument type: F.M. pressure unit
- Type of mounting: Tripod on sea bed
- Record duration: 10 min.
- Record interval: 3 hr.

FORM AND MEDIUM OF DATA
- Original data: Frequency modulated magnetic tape.
- Processed data: Listings of Tucker-Draper statistics as printout or on digital magnetic tape.
- Analysed data: Most standard analysis presentations.

NOTES

Data collected by:
Institute of Oceanographic Sciences, U.K.

Details of wave data from Scarweather Bank and Port Talbot
(extracted from RNODC catalogue of Wave Data, 1979)

TABLE 5

Ray tracking: Range of water depths, wave periods and offshore wave directions

Depth (m)	For direction of 260° at boundary				
	Wave period, Tz (s)				
	4	6	8	10	12
CD + 1.00			*		
CD + 5.25		*	*	*	
CD + 9.50			*		

Direction (0°)	For depth of CD + 5.25m (only)				
	Wave period, Tz (s)				
	4	6	8	10	12
270			*		
260			*		
250			*		
240			*		
230			*		
220			*		
170		*			
160	*	*	*		
150		*			

TABLE 6

(a) Angles of computed wave incidence for wave approach directions between 220° and 270° in relation to beach alignment measured at low water mark.
(b) Correlations and significance levels for beach alignment (x) v computed wave incidence (y) for each water level.

(a)

Beach		Computed Wave Incidence(°)					
Section	Alignment (°)	LW*	Diff	MW*	Diff	HW*	Diff
C	32	33.77±1.71	+1.8	35.08±2.23	+3.1	35.48±2.48	+3.5
E	40	40.72±1.48	+0.7	38.95±1.76	-1.0	39.68±1.61	-0.3
G	48	47.37±1.69	-0.6	46.30±2.74	-1.7	45.90±3.04	-2.1
L	58	56.95±1.43	-1.0	56.02±2.07	-2.0	55.75±2.27	-2.2
N	60	63.25±2.01	+3.3	60.80±2.86	+0.8	60.53±2.44	+0.5
P	70	71.42±0.21	+1.4	69.03±0.97	-1.0	67.70±0.58	-2.3
R	63	63.53±0.11	+0.5	66.07±1.68	+3.1	65.90±1.63	+2.9
T	67	70.68±0.71	+3.7	63.78±2.20	-3.2	64.90±3.09	-2.1
V	69	70.00±1.02	+1.0	70.0±2.55	+1.0	68.93±2.98	-0.1
X	69	70.60±0.58	+1.6	75.73±1.41	+6.7	76.48±1.75	+7.5
Z	57	80.55±2.24	+23.6	82.84±2.86	+25.5	75.98±4.14	+19.0

(b)

	LW*			MW*			HW*		
	Corr	Sig	y =	Corr	Sig	y =	Corr	Sig	y =
C-T n=6	.993	.001	1.031x-0.510	.981	.001	0.929x+3.259	.986	.001	0.920x+4.115
C-V n=7	.994	.001	1.024x-0.189	.982	.001	0.951x+2.268	.987	.001	0.932x+3.604
C-X n=8	.994	.001	1.025x-0.221	.970	.001	1.006x-0.153	.972	.001	0.993x+0.924
C-Z n=9	.882	.001	1.018x+2.249	.851	.001	0.995x+2.399	.891	.001	0.987x+2.965

*LW, MW, HW = 1.0, 5.25 and 9.50m above CD respectively.

TABLE 7

Computed wave energy coefficients (E) and relative wave energy levels (E/E_L) for 3 offshore wave directions - (250^o, 260^o, 270^o) and 3 water levels (LW, MW, HW*) for beach sections C to Z. Means and standard deviations of E and E/E_L are denoted by μ and σ respectively.

Section Line	Computed relative wave energy									E (m^2)		E/E_L	
	Waves from: 250^o offshore			260^o offshore			270^o offshore						
	LW	MW	HW	LW	MW	HW	LW	MW	HW	μ	σ	μ	σ
C	.595	.555	.489	.456	.409	.367	.328	.276	.253	.414	.113	.520	.142
E	.755	.530	.452	.591	.413	.354	.426	.295	.253	.452	.147	.568	.185
G	1.033	.759	.694	.812	.614	.567	.587	.464	.432	.662	.176	.832	.221
L	1.009	.922	.799	.902	.812	.704	.763	.672	.582	.796	.126	1.000	.158
N	.777	.829	.777	.672	.717	.695	.550	.585	.584	.687	.093	.863	.117
P	1.683	1.135	.814	1.684	1.123	.799	1.587	1.050	.739	1.179	.360	1.481	.452
R	.589	.626	.612	.573	.596	.582	.527	.537	.522	.574	.035	.721	.044
T	1.116	.777	.663	1.081	.752	.622	.988	.637	.550	.795	.200	.999	.251
V	.421	.457	.400	.434	.448	.382	.423	.417	.344	.414	.033	.520	.041
X	.119	.225	.304	.116	.207	.295	.106	.199	.272	.205	.073	.258	.092
Z	.259	.542	.561	.248	.522	.541	.225	.478	.495	.430	.134	.540	.168

*LW, MW, HW - Water levels 1.0, 5.25 & 9.50m above CD, respectively

E/E_L - Normalised wave energy energy with respect to Section L (approx Port Talbot)

TABLE 8

Computed wave energy coefficients (E) and relative wave energy levels (E/E_L) for 3 offshore wave directions - (220^o, 230^o, 240^o) and 3 water levels (LW, MW, HW*) for beach sections C to Z. Means and standard deviations of E and E/E_L are denoted by μ and σ respectively.

Section Line	Computed relative wave energy												
	Waves from:									E (m^2)		E/E_L	
	220^o offshore			230^o offshore			240^o offshore						
	LW	MW	HW	LW	MW	HW	LW	MW	HW	μ	σ	μ	σ
C	.955	.910	.753	.859	.821	.694	.734	.698	.602	.781	.108	1.013	.139
E	1.081	.754	.622	1.016	.712	.594	.903	.634	.535	.761	.184	.986	.239
G	1.442	1.013	.885	1.368	.970	.863	1.226	.882	.797	1.050	.223	1.362	.289
L	1.048	.972	.829	1.085	1.007	.865	1.072	.990	.855	.969	.092	1.256	.119
N	.892	.931	.781	.892	.943	.823	.853	.908	.822	.872	.052	1.131	.068
P	1.155	.792	.592	1.402	.955	.704	1.585	1.075	.781	1.005	.313	1.303	.406
R	.453	.530	.511	.525	.591	.574	.572	.634	.610	.554	.051	.719	.067
T	.868	.692	.581	1.002	.760	.642	1.088	.790	.671	.788	.160	1.021	.207
V	.275	.355	.339	.337	.407	.378	.388	.442	.399	.369	.046	.479	.059
X	.094	.182	.238	.107	.206	.273	.116	.221	.296	.193	.069	.250	.089
Z	.221	.451	.453	.245	.505	.514	.258	.536	.551	.451	.127	.538	.165

*LW, MW, HW - Water levels 1.0, 5.25, 9.50m above CD respectively

E/E_L - Normalised wave energy with respect to that from offshore wave directions of 250^o - 270^o arriving at Section L (approx Port Talbot)

TABLE 9

Maximum height range for beach sections during period Sept/Oct 1975 to April/May 1977.

Section Line	Height range (cm)		
	Lower beach*	Upper beach*	Average
C	40	40	40
E	55	45	50
G	55	40	47.5
L	45	60	52.5
N	55	60	57.5
P	110	60	85
R	65	40	52.5
T	70	70	70
V	90	110	100
X	95	70	82.5
Z	80	80	80

* Lower beach = below zero OD (ie approximately mean sea level)

* Upper beach = between zero and +3.0m OD (ie excluding pebble/cobble storm beach zone, so only sand area is considered)

TABLE 10

Correlation coefficients and significance levels (in brackets) for height range of different beach zones v computed wave energy for low, mid- and high water levels.
(a) Sections C to T (n = 6). (b) Sections C to V (n = 7).

Offshore Direction of Wave Approach													
Beach Zone	240°			250°			260°			270°			
	Water Level*												
	LW	MW	HW	LW	MW	HW	LW	MW	HW	LW	MW	HW	
Lower	.696(.1)	-	-	.812(.02)	.674(.1)	-	.873(.01)	.774(.05)	-	.898(.01)	.827(.02)	.685(.1)	a
	-	-	-	-	-	-	.595(.1)	-	-	.683(.05)	.646(.1)	-	b
Upper	-	-	-	-	.626(.1)	-	-	.655(.1)	.659(.1)	-	.640(.1)	.665(.1)	a
	-	-	-	-	-	-	-	-	-	-	-	-	b
Average	.705(.1)	-	-	.855(.01)	.783(.02)	-	.921(.01)	.864(.01)	.750(.05)	.948(.001)	.898(.01)	.800(.02)	a
	-	-	-	-	-	-	-	-	-	-	-	-	b

*LW, MW, HW = 1.0, 5.25 and 9.5m above CD, respectively. T_Z = 8s: H_S = 1m

No correlations significant with offshore approach angles of 220° and 230°. No correlations significant at any level for entire beach (Sections C to Z) for any offshore wave direction (220° to 270°) or beach zone.

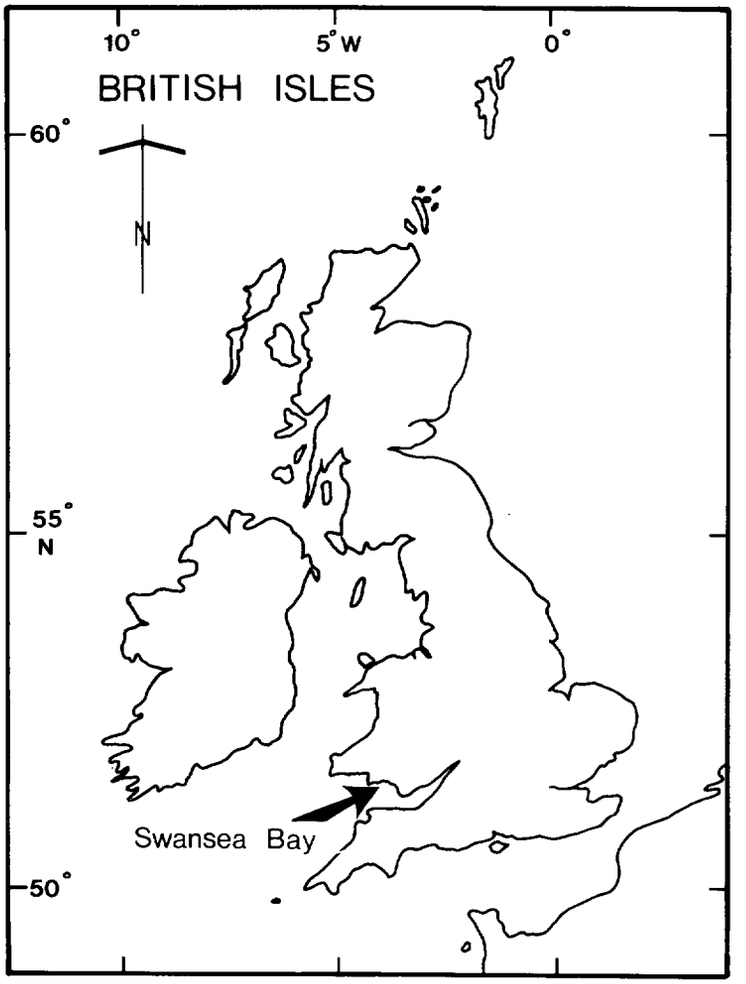

Figure 1. Study area

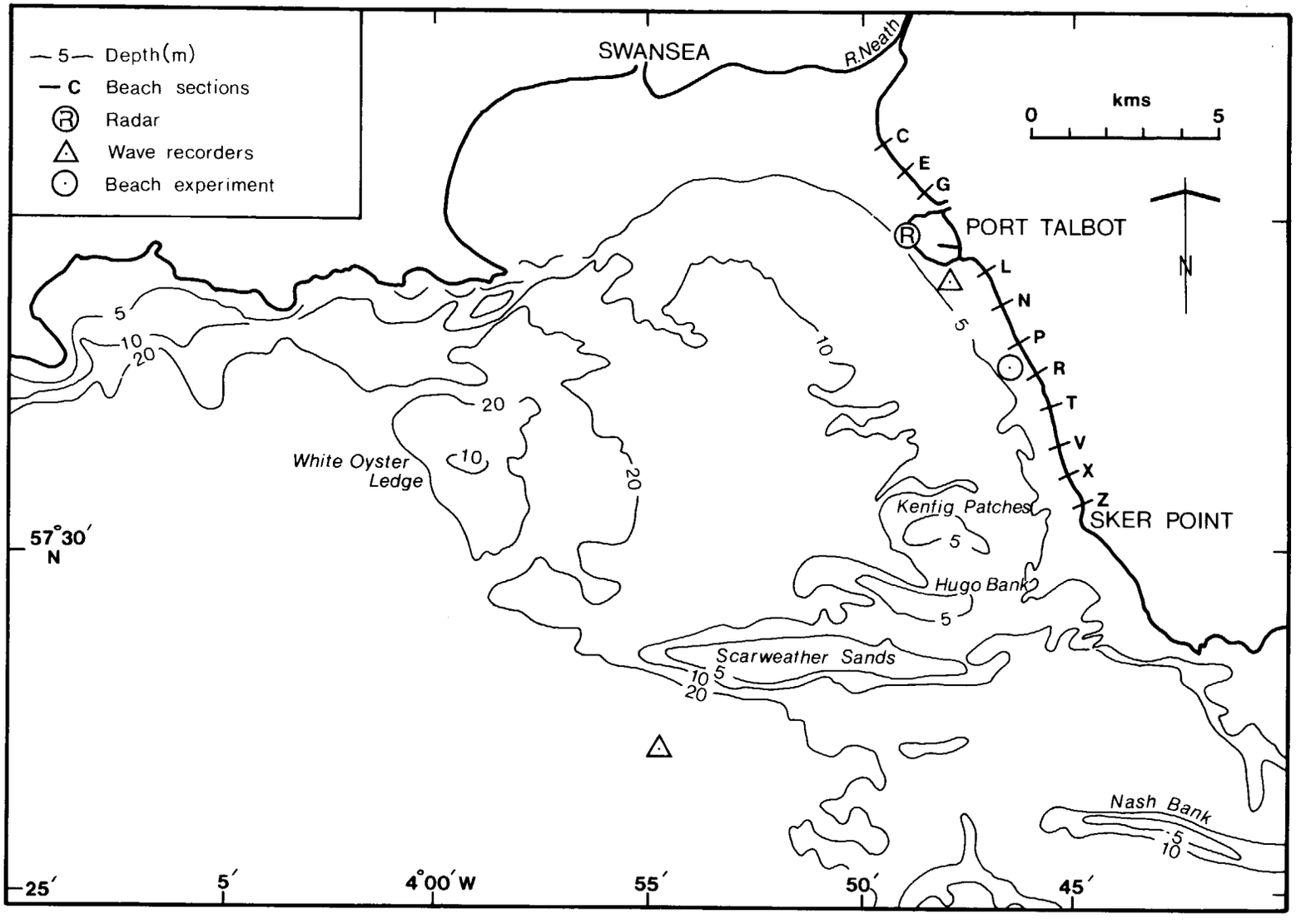

Figure 2 Swansea Bay in the Bristol Channel showing the location of wave recorders, the radar installation, beach sections and the site of the 1976 and 1977 beach experiments. The location of the offshore banks are also shown.

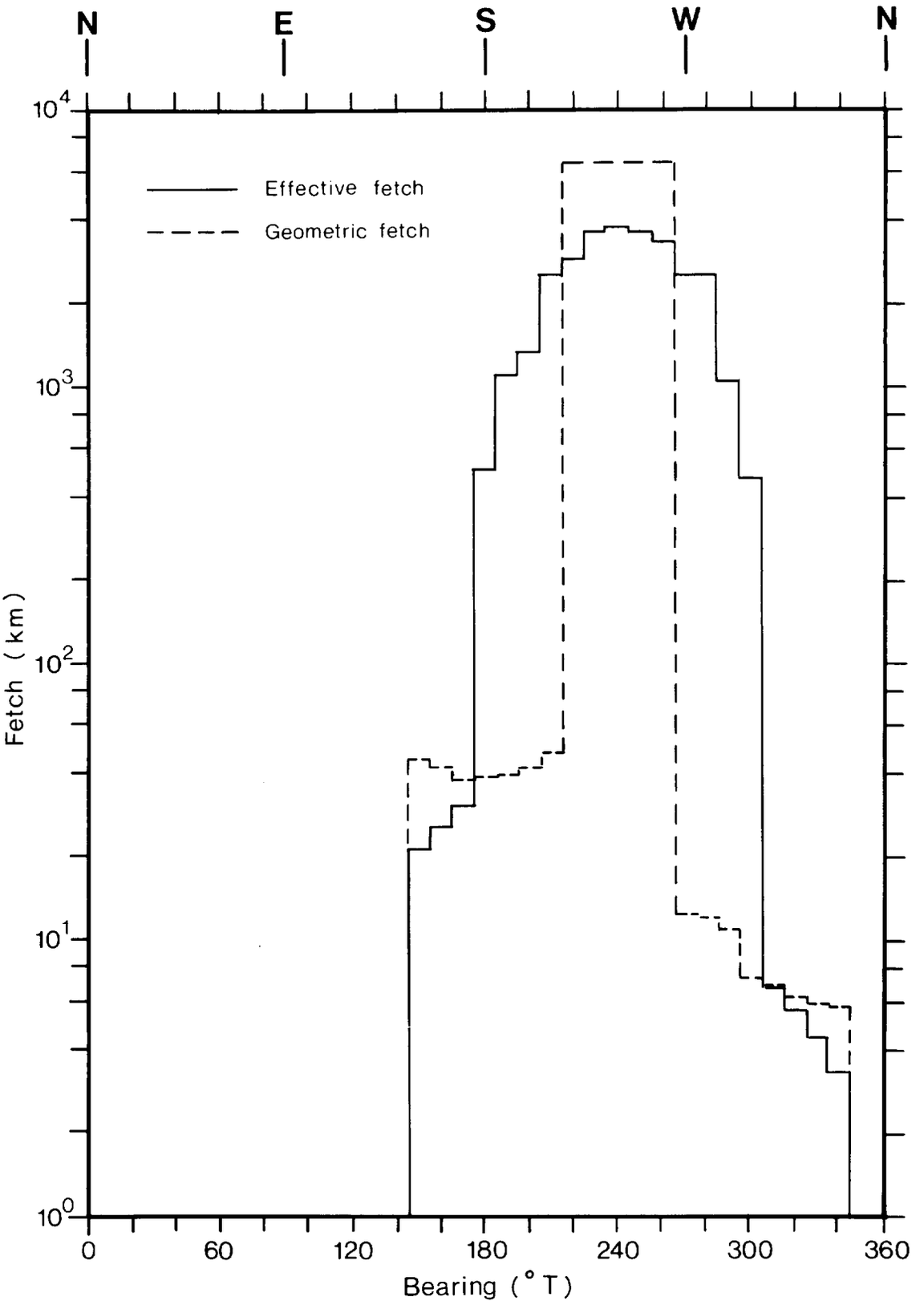

Figure 3. Effective fetch characteristics at Port Talbot in Swansea Bay illustrating the extent to which its wave climate is controlled by its 'open fetch' from the N Atlantic. Bearings are in degrees (True) from Port Talbot.

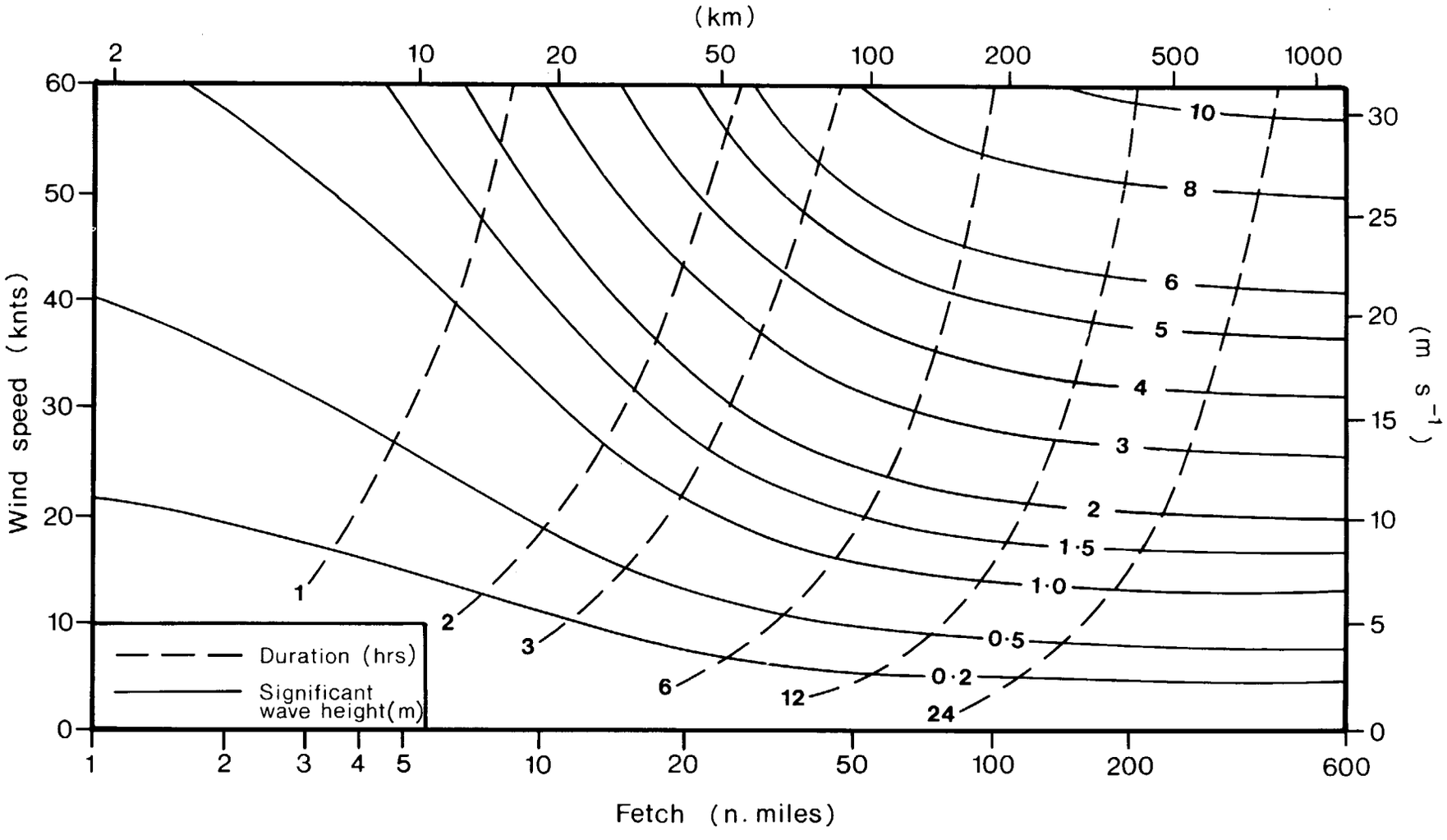

Figure 4 Wave height prediction curves (after Darbyshire and Draper, 1963) used to estimate significant wave heights (H_s) for different wind speeds (Tables 2 and 3) from the effective fetch characteristics shown in Figure 3.

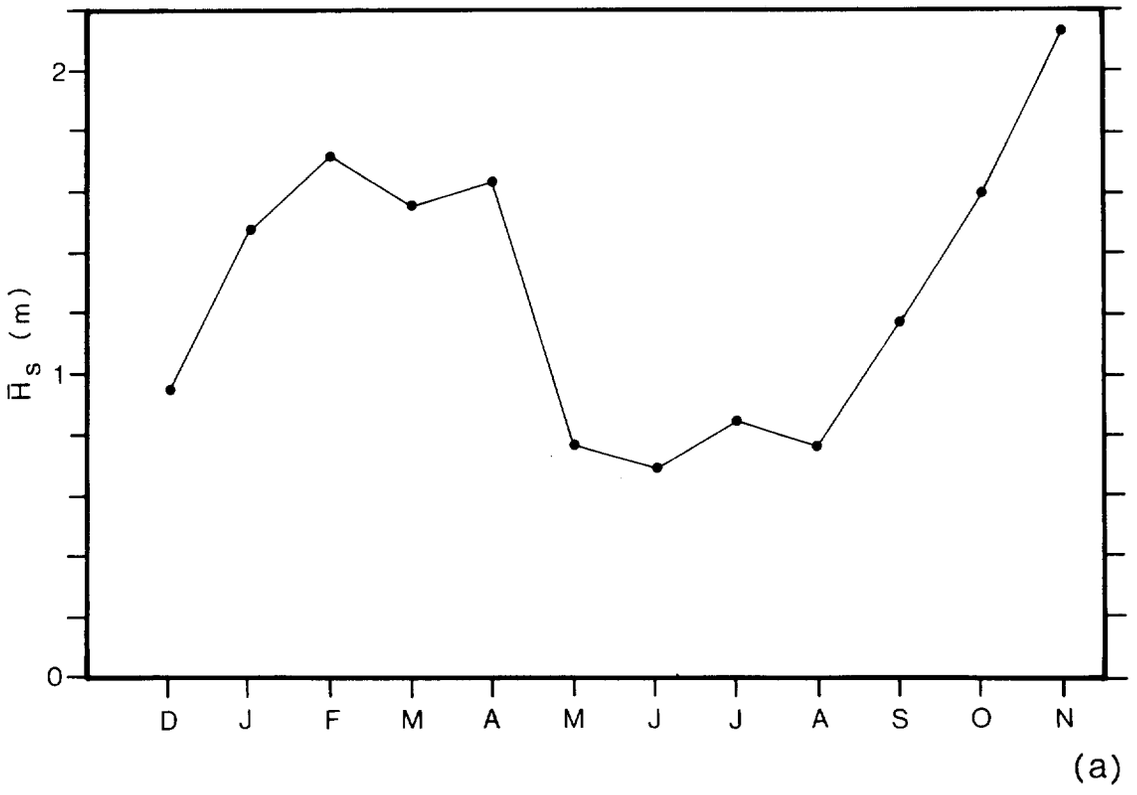

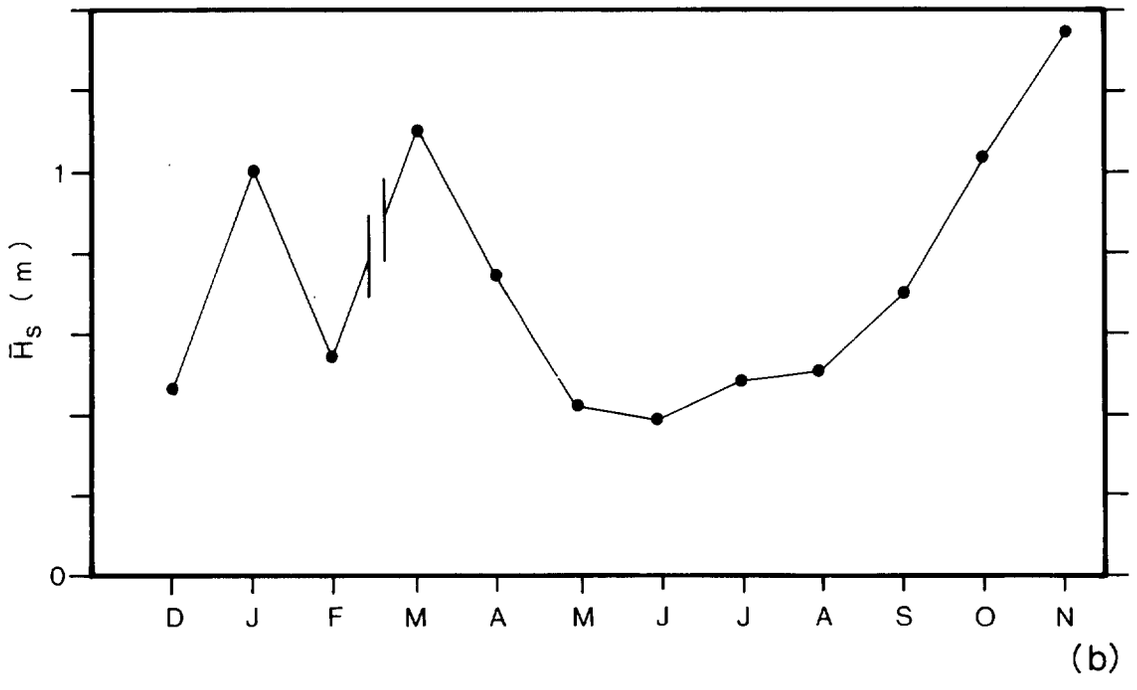

Figure 5 Seasonal variations of the monthly mean significant wave heights ($\bar{H}_s$) at (a) the Scarweather Light Vessel and (b) at Port Talbot. Note difference in $\bar{H}_s$ scale. (After Fortnum and Hardcastle, 1979 a,b). Note: (a) and (b) correspond to the periods December 1976 - November 1977 and December 1975 - February 1976/March 1977 - November 1977 respectively.

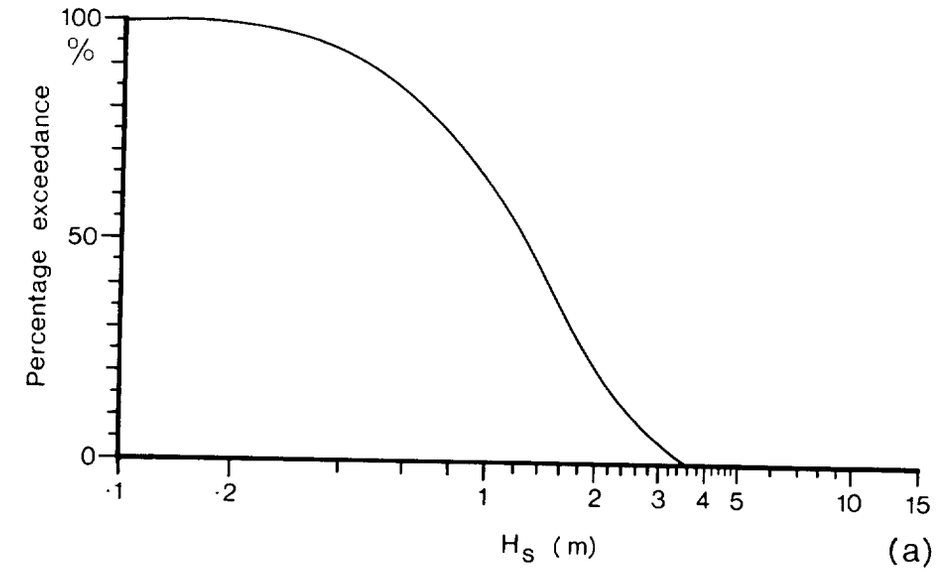

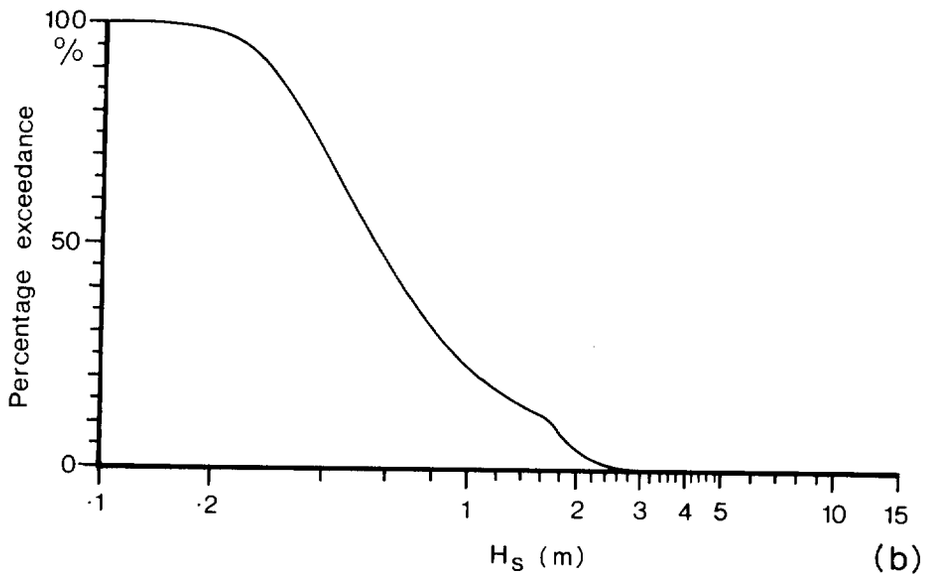

Figure 6 Winter (a) and Summer (b) wave height (H_s) exceedance curves for waves measured near the Scarweather Light Vessel (after Fortnum and Hardcastle, 1979b). Note: (a) and (b) correspond to periods December 1976 - February 1977 and June - August 1977 respectively.

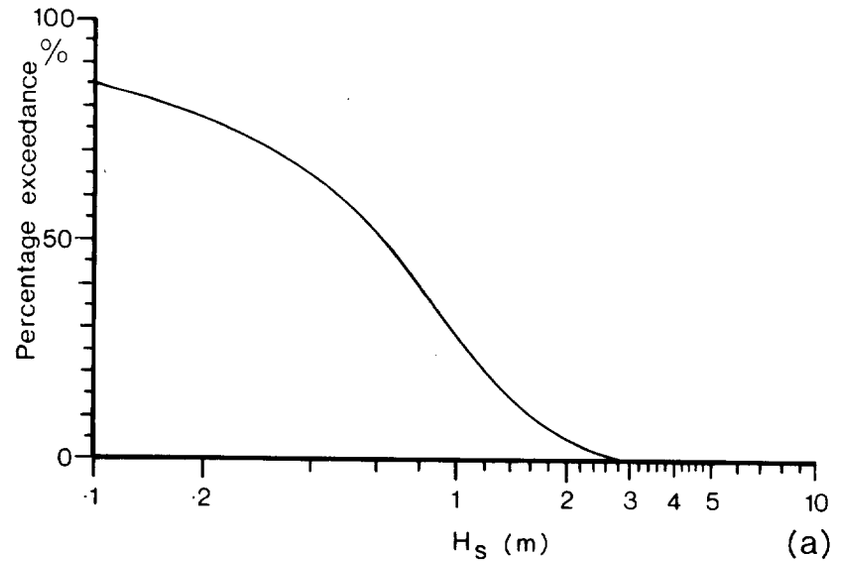

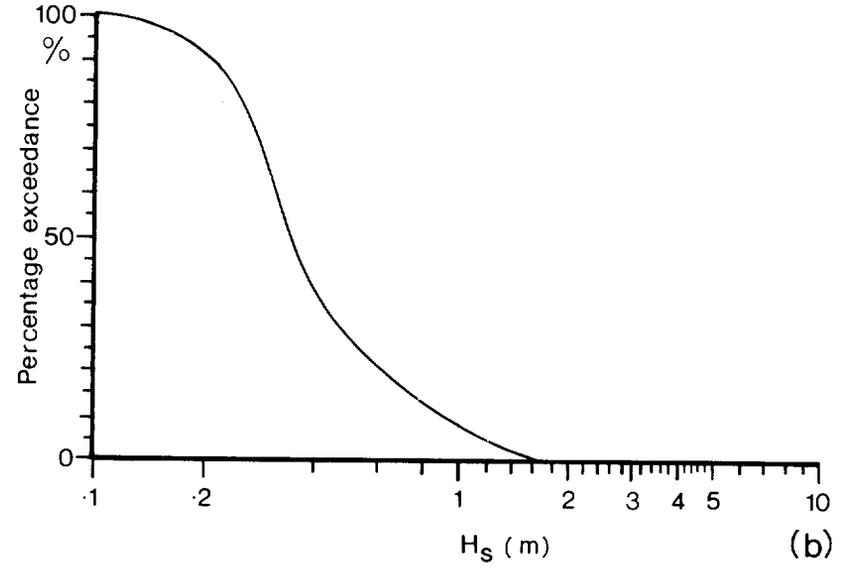

Figure 7 Winter (a) and Summer (b) wave height (H_s) exceedance curves for waves measured at Port Talbot (after Fortnum and Hardcastle, 1979a). Note: (a) and (b) correspond to the periods December 1975 - February 1976 and June - August 1977 respectively.

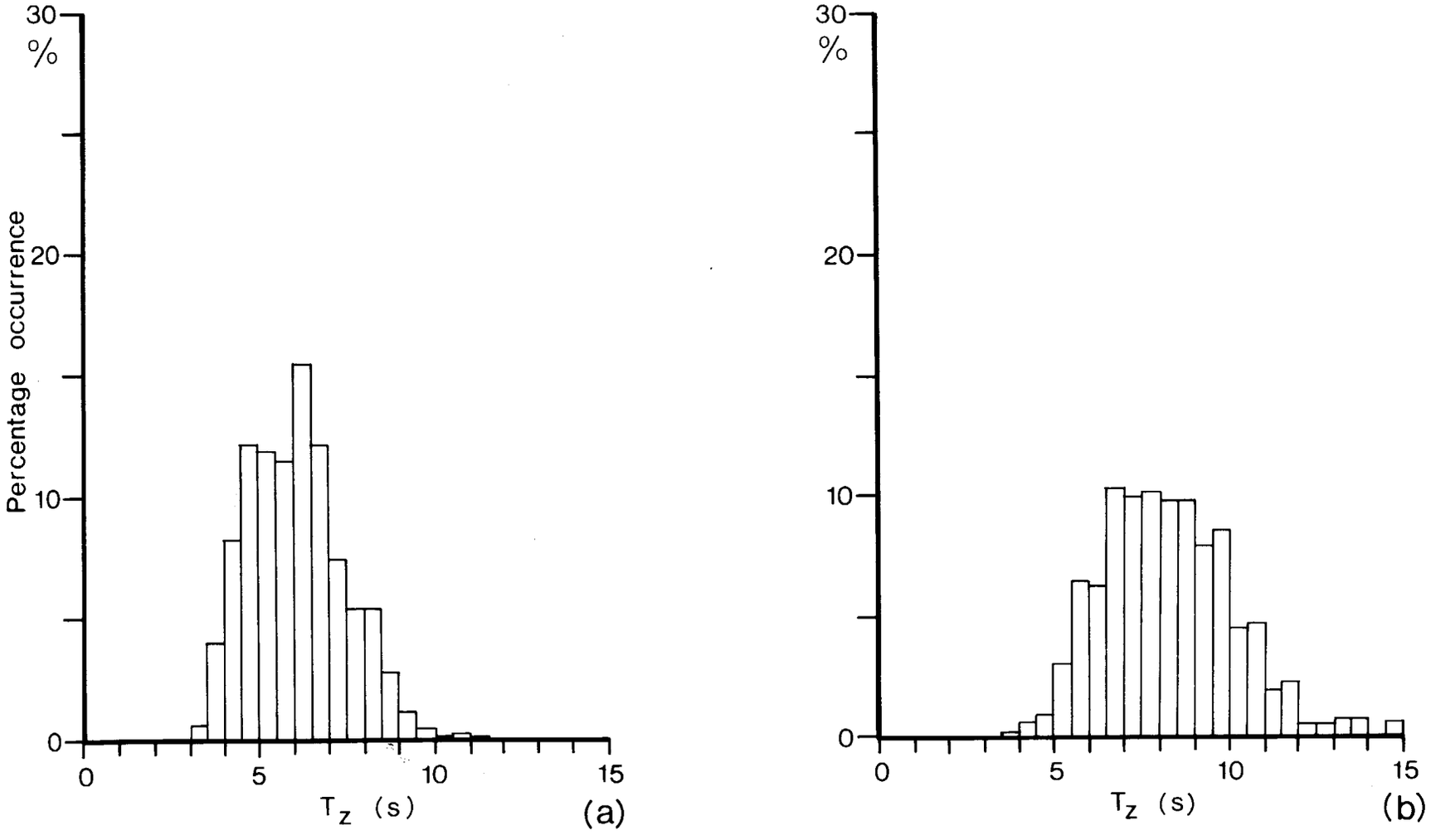

Figure 8 Summer (a) and winter (b) wave period (T_z) frequency histograms for waves recorded at the Scarweather Light Vessel (after Fortnum and Hardcastle, 1979b). Note: (a) and (b) correspond to periods December 1976 - February 1977 and June - August 1977 respectively.

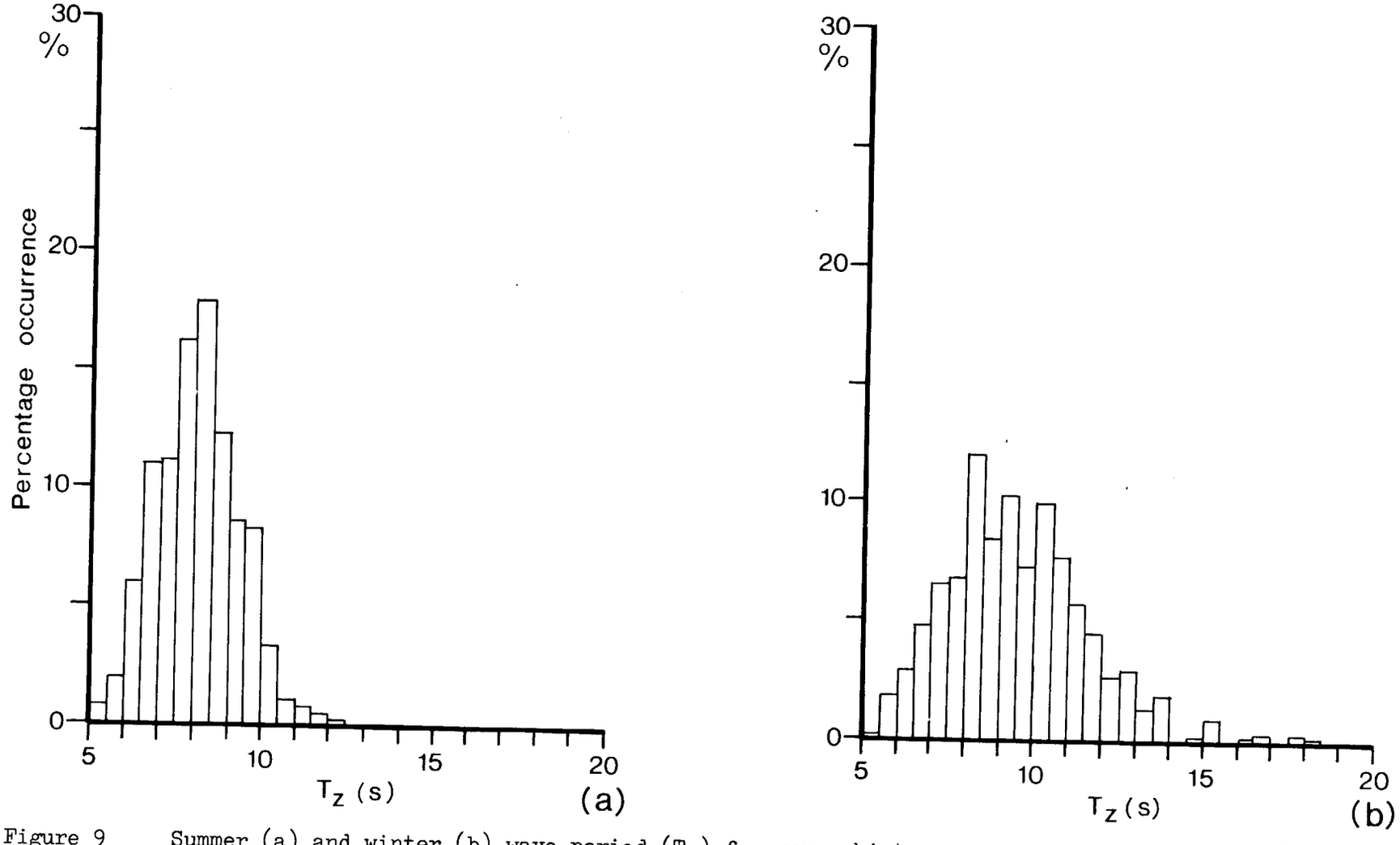

Figure 9 Summer (a) and winter (b) wave period (T_z) frequency histograms for waves recorded at Port Talbot (after Fortnum and Hardcastle, 1979a). Note: (a) and (b) correspond to the periods December 1975 - February 1976 and June - August 1977 respectively.

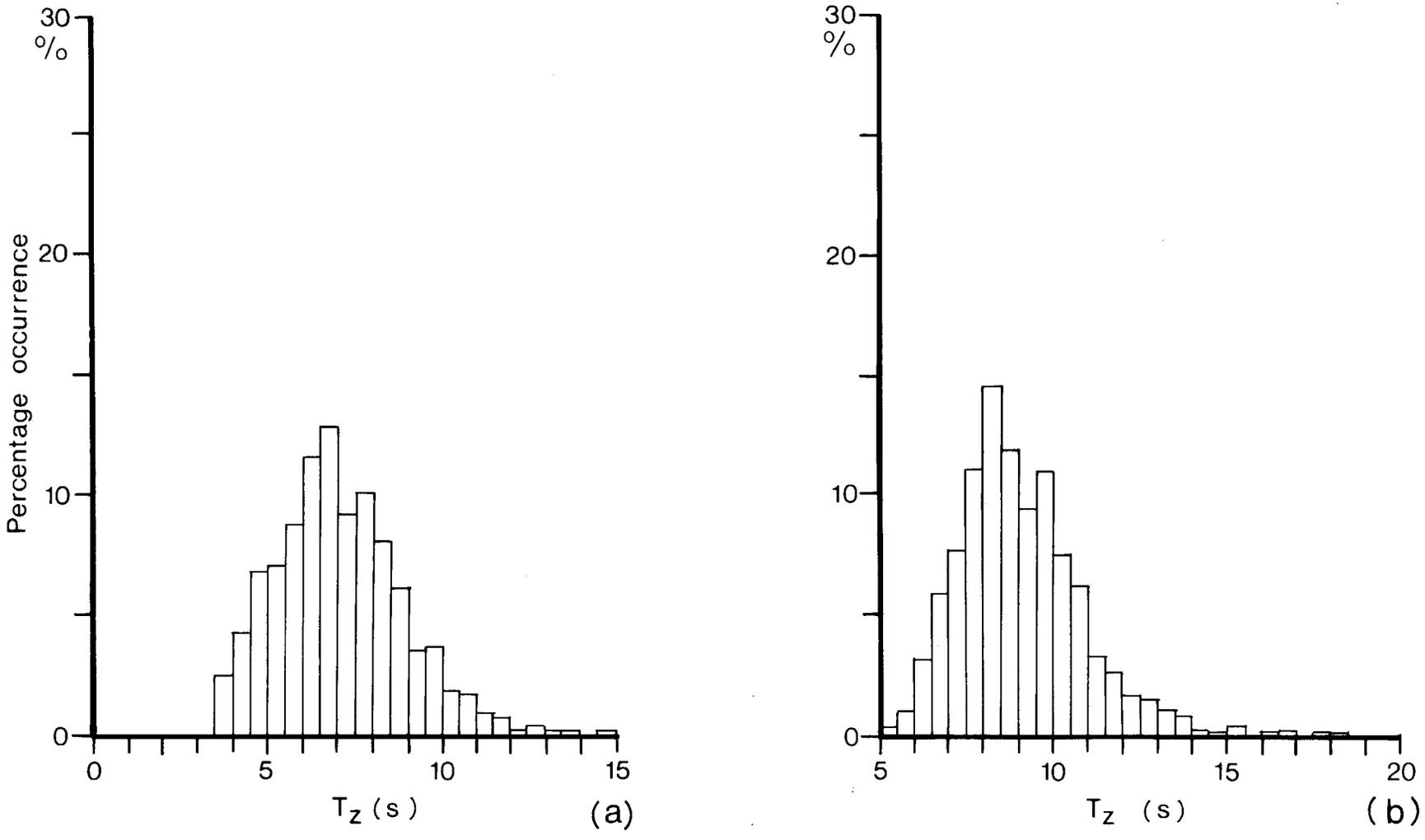

Figure 10 Annual wave period (T_z) frequency histograms for waves recorded at (a) the Scarweather Light Vessel and (b) at Port Talbot (after Fortnum and Hardcastle, 1979a, b). Note: (a) and (b) correspond to the periods December 1976 - november 1977 and December 1975 - February 1976/March 1977 - November 1977 respectively.

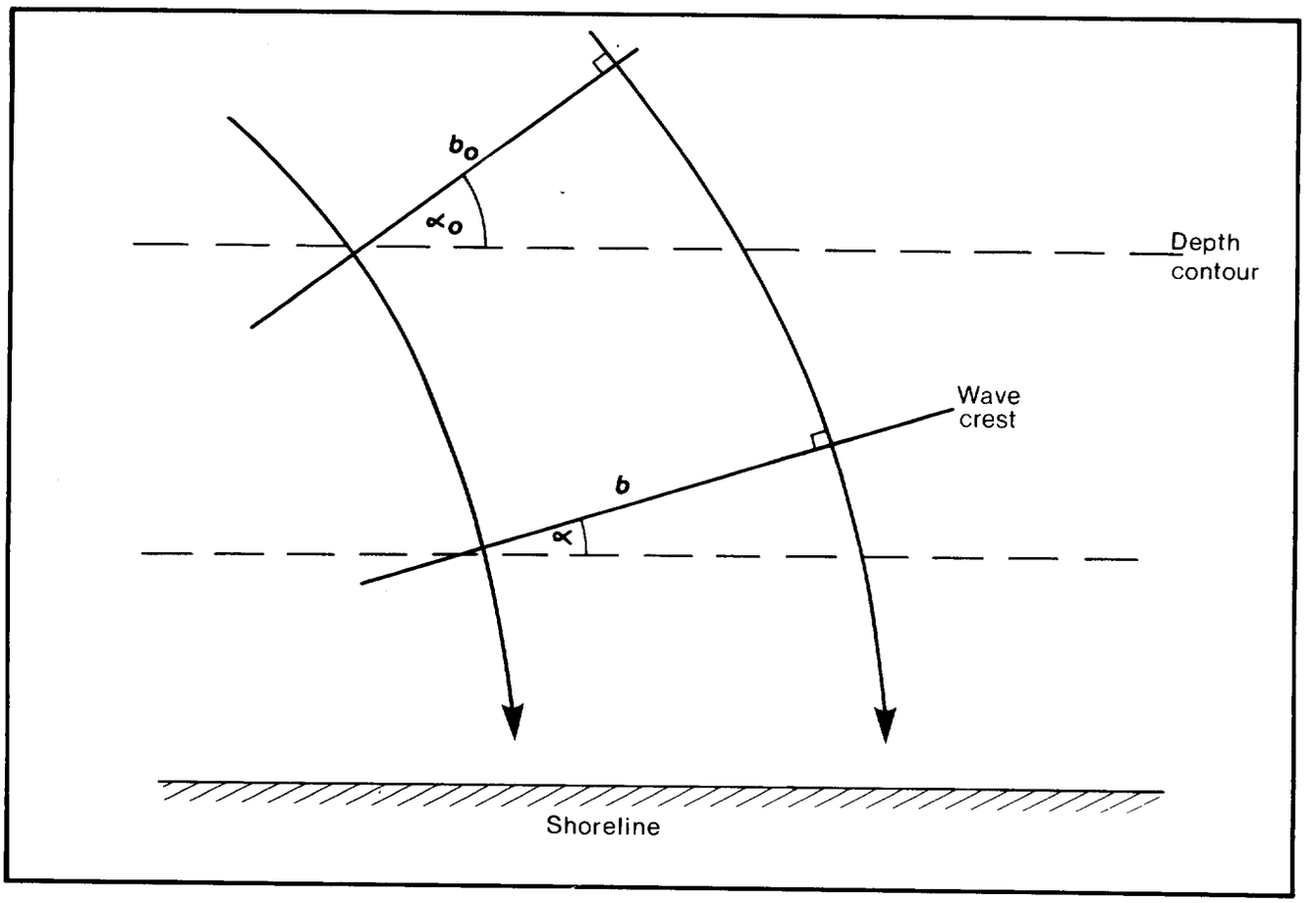

Figure 11 Schematic presentation of wave refraction processes.

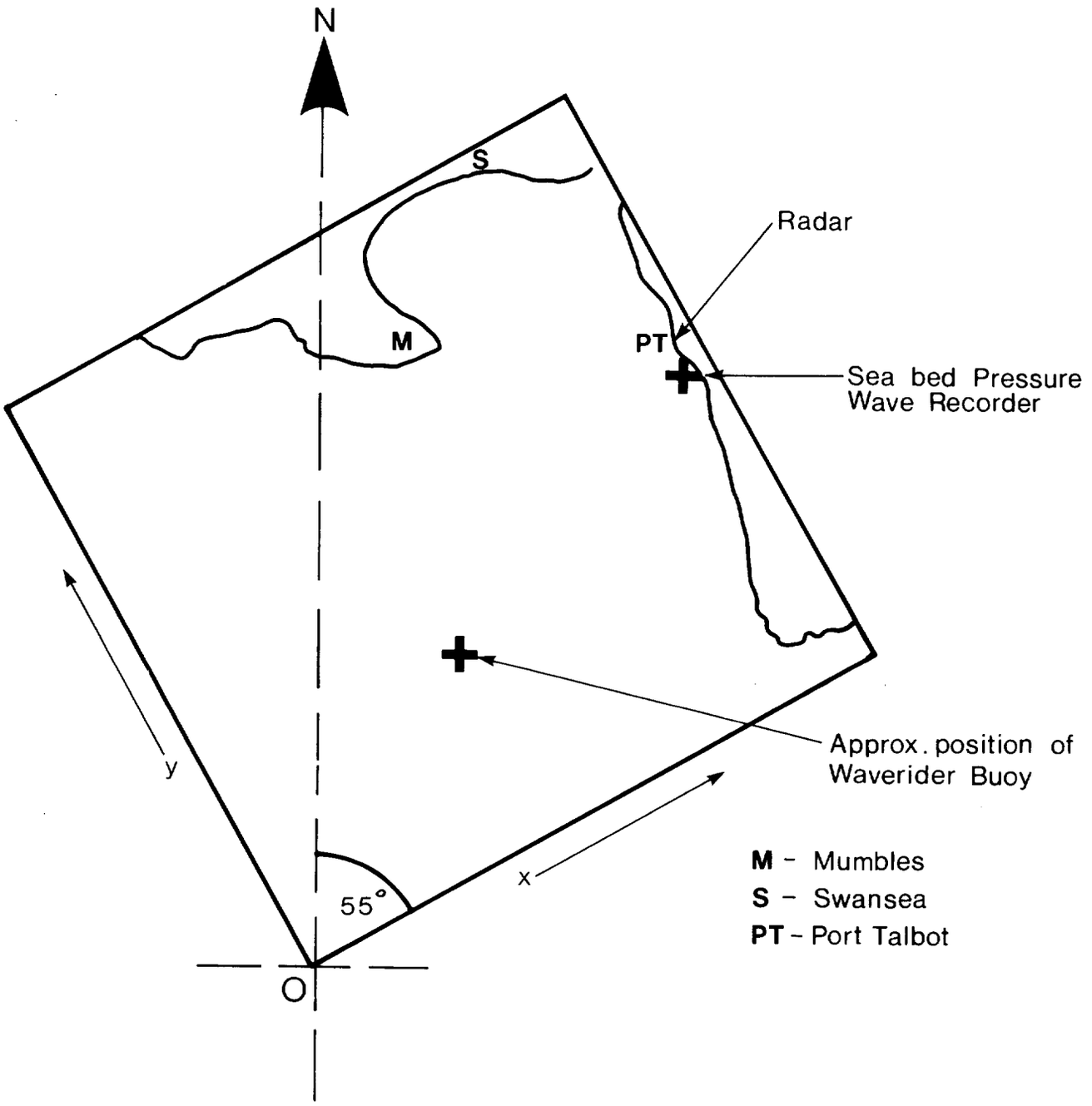

Origin (O) at: 3° 58.00′ W 51° 21.00′ N
Overall dimensions of grid are 25×25 km made up of 50×50 elements having dimensions 500×500 m.

Figure 12 Area covered by IOS wave refraction grid.

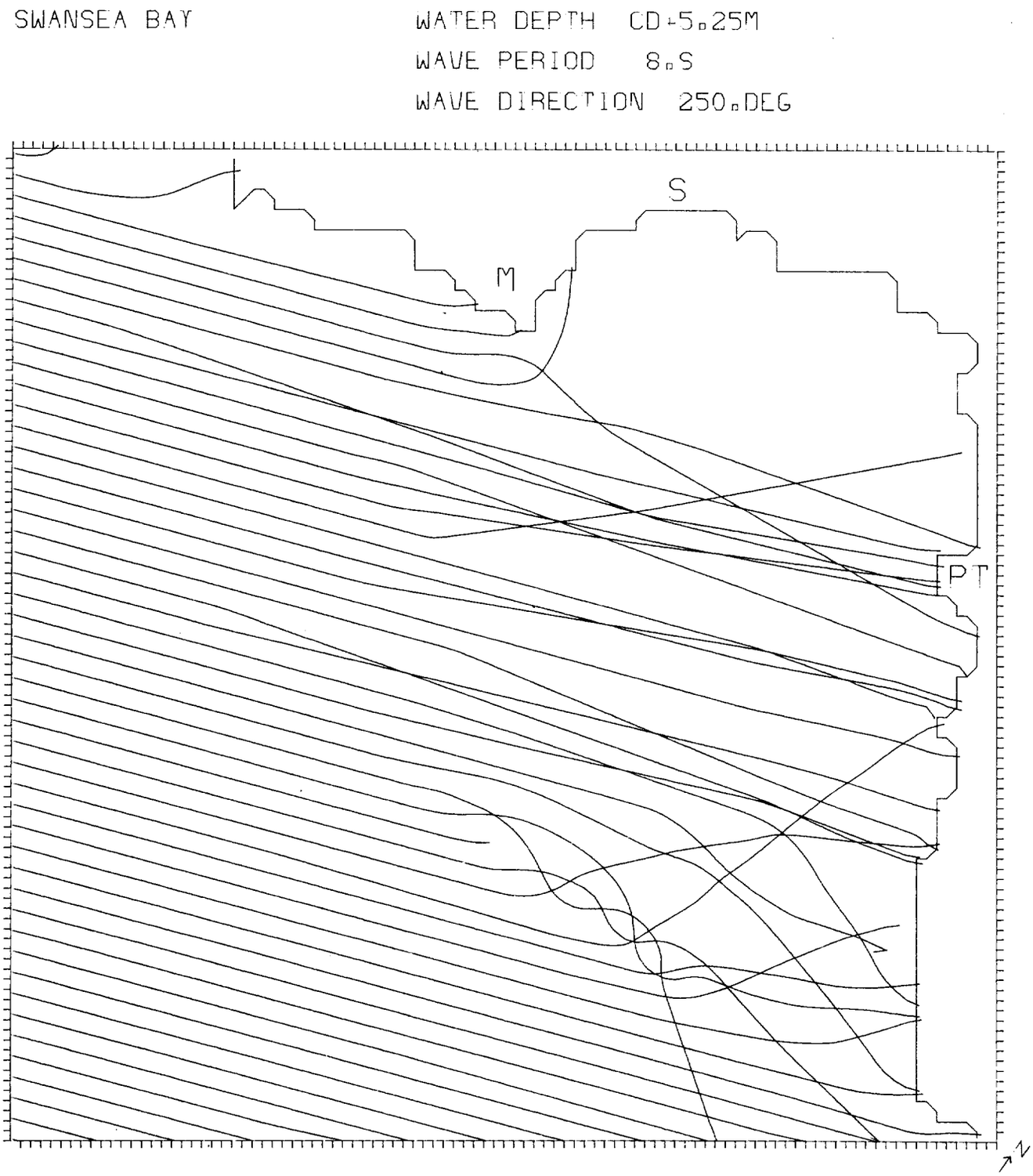

Figure 13 Typical wave refraction diagrams for an offshore wave approach direction of 250° and a water depth of CD + 5.25m (roughly mid-tide level).

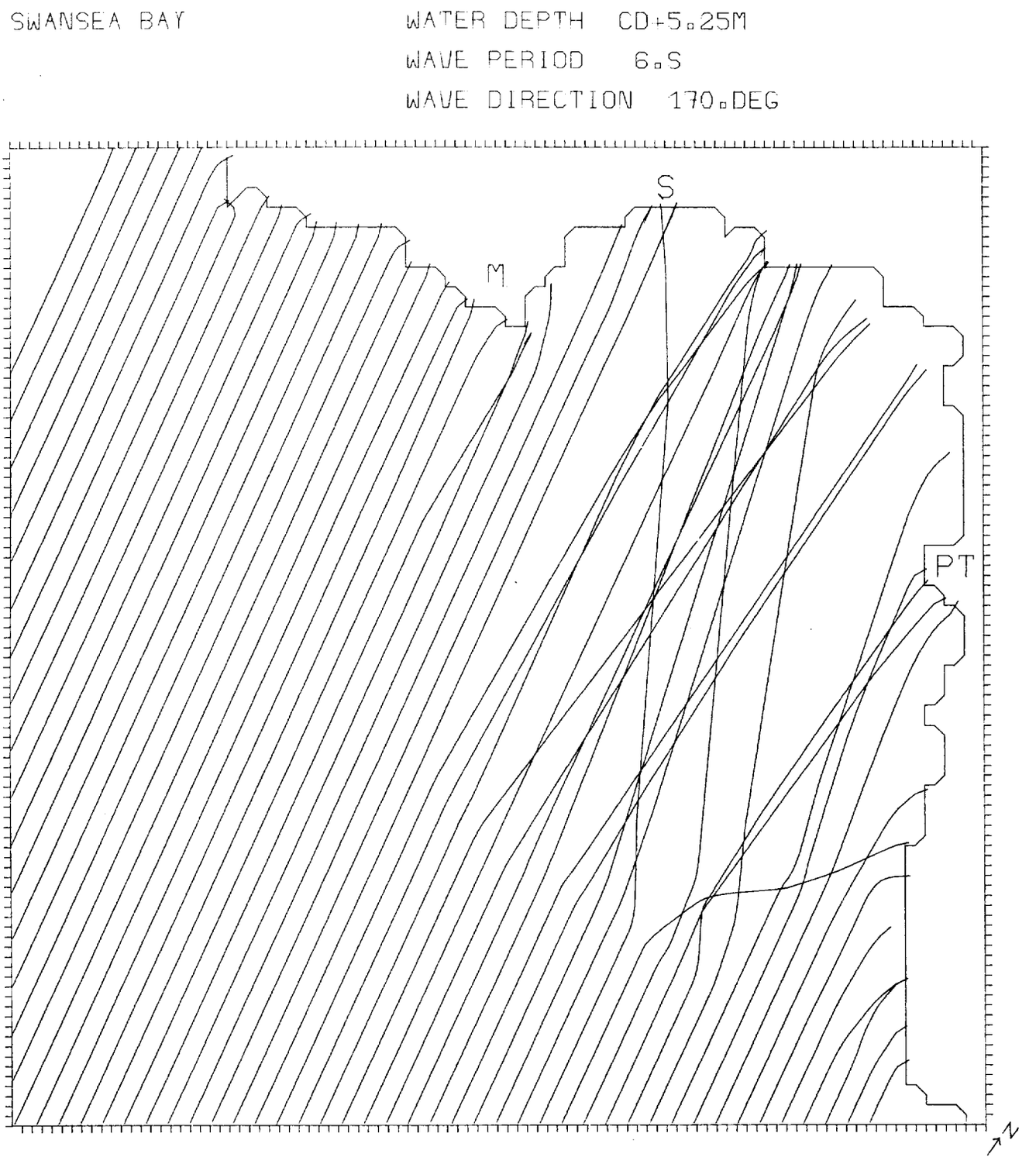

Figure 14 Typical wave refraction diagram for an offshore wave approach direction of 170° and a water depth of CD + 5.25m (roughly mid-tide level).

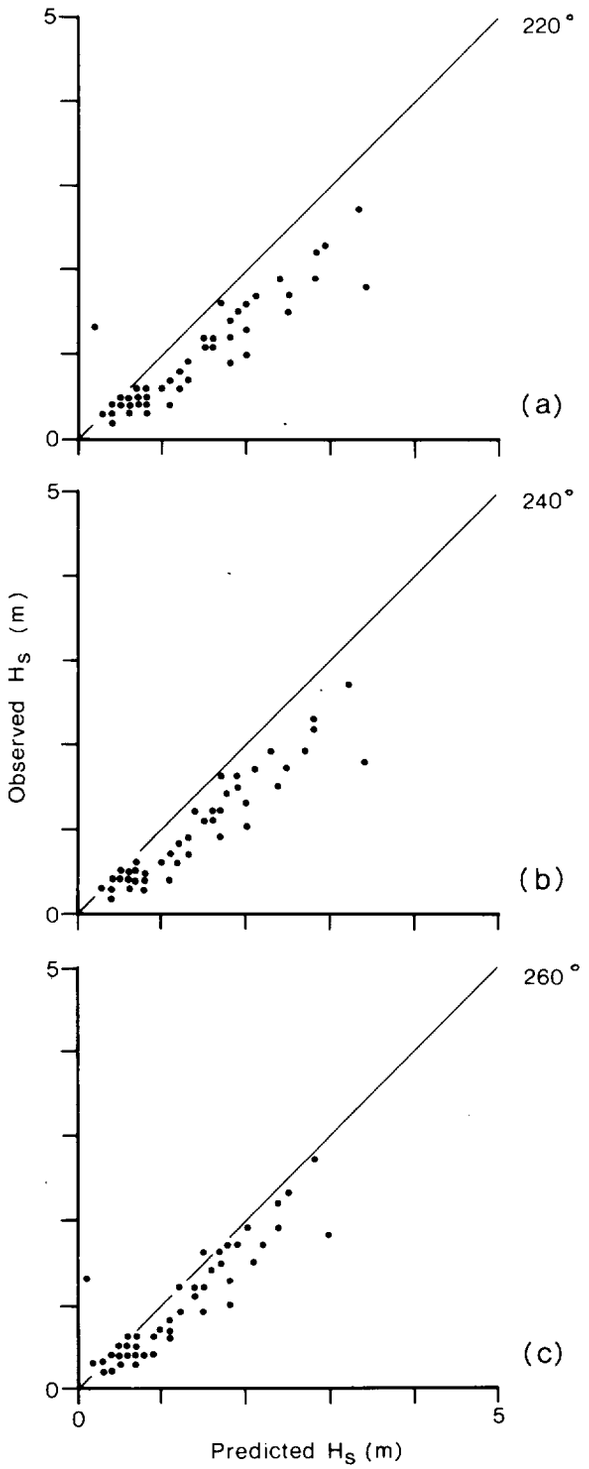

Figure 15 Comparisons of observed and predicted wave heights (H_s) at Port Talbot for offshore wave approach directions of (a) 220°, (b) 240° and (c) 260°. A Pierson-Moskowitz spectrum was used to specify the offshore wave climate in terms of measured H_s and T_z values from the wave recorder near the Scarweather Light Vessel (see Appendix B for details).

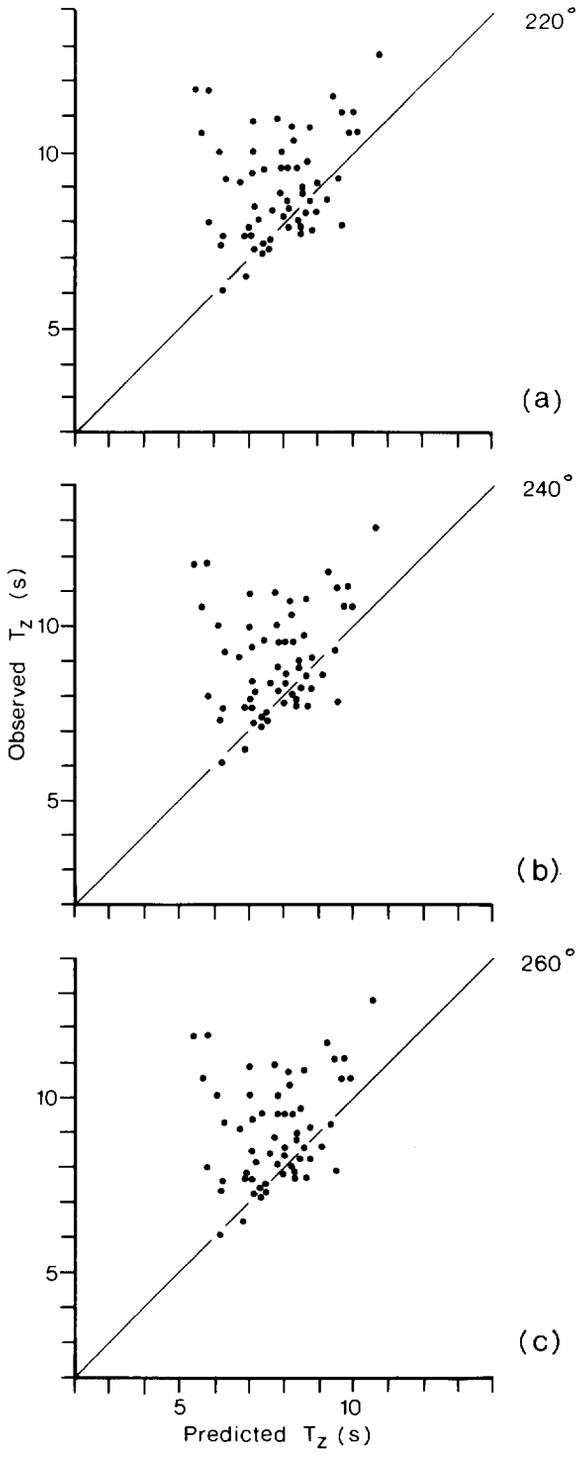

Figure 16 Comparisons of observed and predicted wave periods (T_z) at Port Talbot for offshore wave approach directions of (a) 220°, (b) 240° and (c) 280°. A Pierson-Moskowitz spectrum was used to specify the offshore wave climate in terms of measured H_s and T_z values from the wave recorder near the Scarweather Light Vessel (see Appendix B for details).

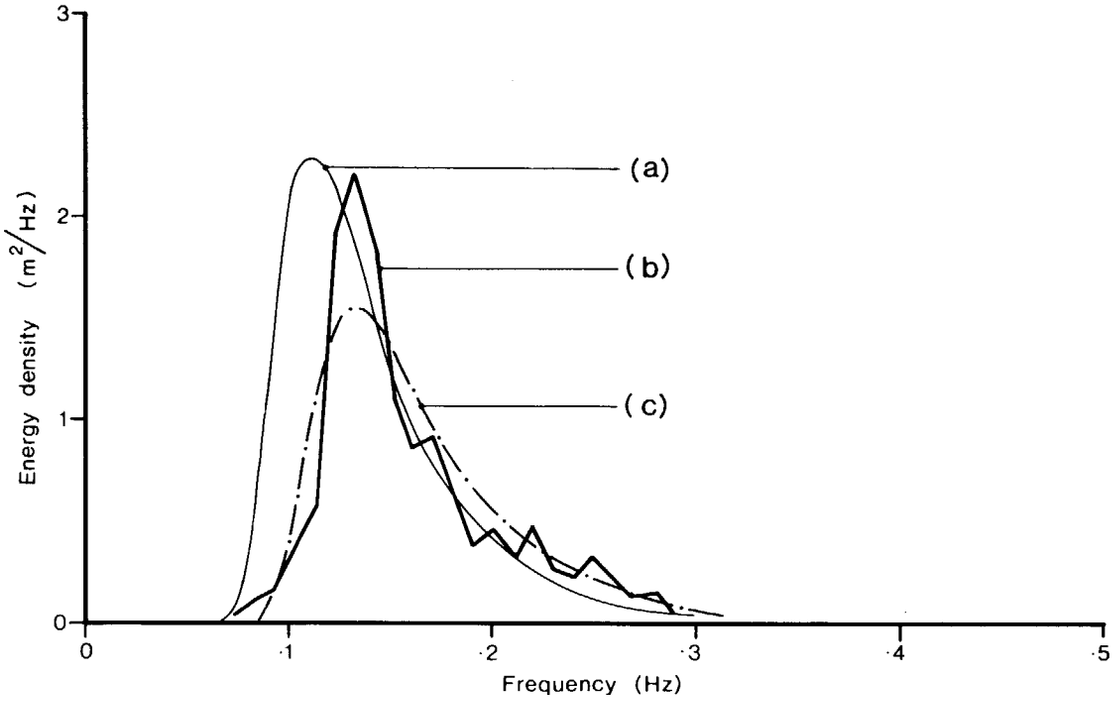

Figure 17 Theoretical and observed wave spectra showing: (a) Pierson-Moskowitz (PM) spectrum (equation B24) evaluated for H_s = 1.70m and T_z = 6.32s; (b) Fast Fourier Transform (FFT) wave spectrum of same record giving H_s = 1.51m and T_z = 5.37s (calculated from FFT spectrum); (c) Pierson-Moskowitz spectrum calculated using FFT values of H_s and T_z.

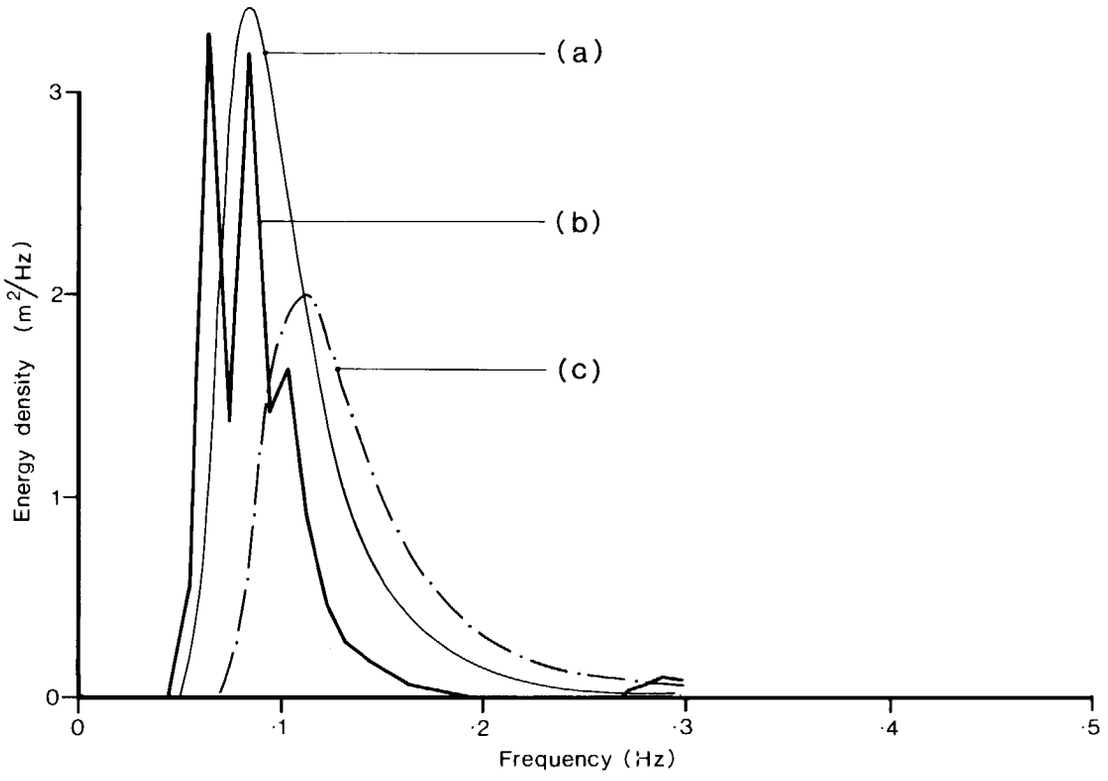

Figure 18. Theoretical and observed wave spectra showing: (a) Pierson-Moskowitz (PM) spectrum (equation B24) evaluated for H_s = 1.80m and T_z = 8.45s; (b) Fast Fourier Transform (FFT) wave spectrum of same record giving H_s = 1.56m and T_z = 5.37s (calculated from FFT spectrum); (c) Pierson-Moskowitz spectrum calculated using FFT values of H_s and T_z.

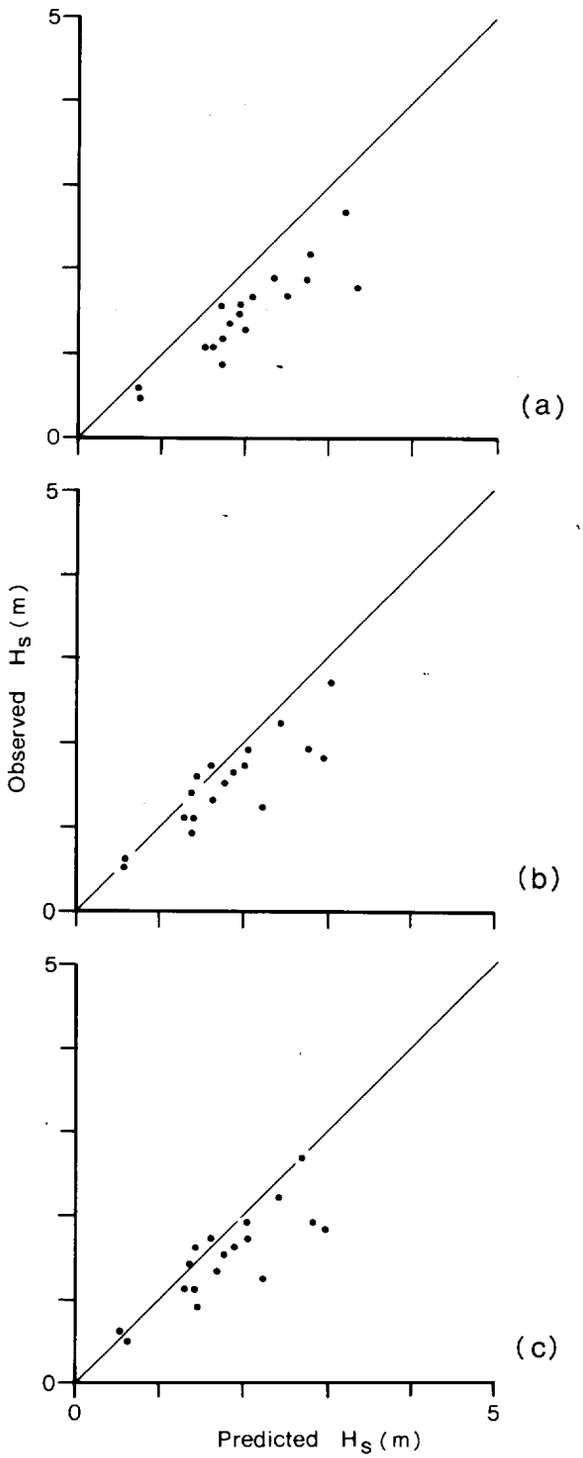

Figure 19. Comparisons of observed and predicted wave heights (H_s) calculated by 3 different methods for an offshore wave approach direction of 240° and showing: (a) Pierson-Moskowitz predictions from measured H_s and T_z values; (b) Pierson-Moskowitz predictions from FFT estimates of H_s and T_z; (c) FFT predictions.

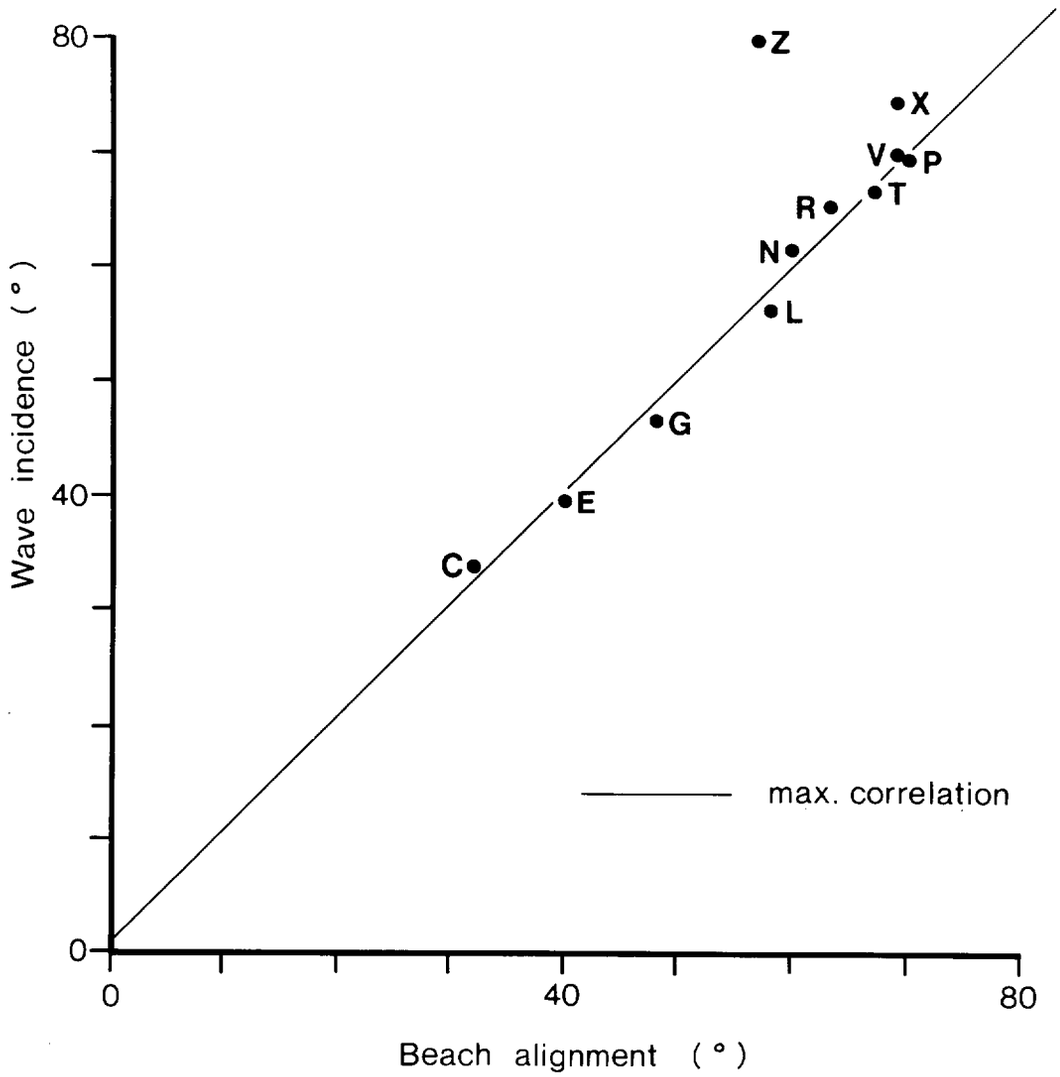

Figure 20 Relation of computed wave incidence to beach alignment at the Low Water level. Wave incidence values were obtained by taking the mean of the values on each section (C to Z in Figure 2) for water levels of 1.0, 5.25 and 9.50m above Chart Datum. The solid line represents that data group which gave the maximum correlation between wave incidence and beach alignment. Details of the various groups examined are:

Sections	No of sections	Correlation Coefficient	
C - T	8	.993	(.834)
C - V	9	.994	(.798)
C - X	10	.988	(.765)
C - Z	11	.879	(.735)

Values of the correlation coefficient at the 1% level of significance are denoted in brackets.

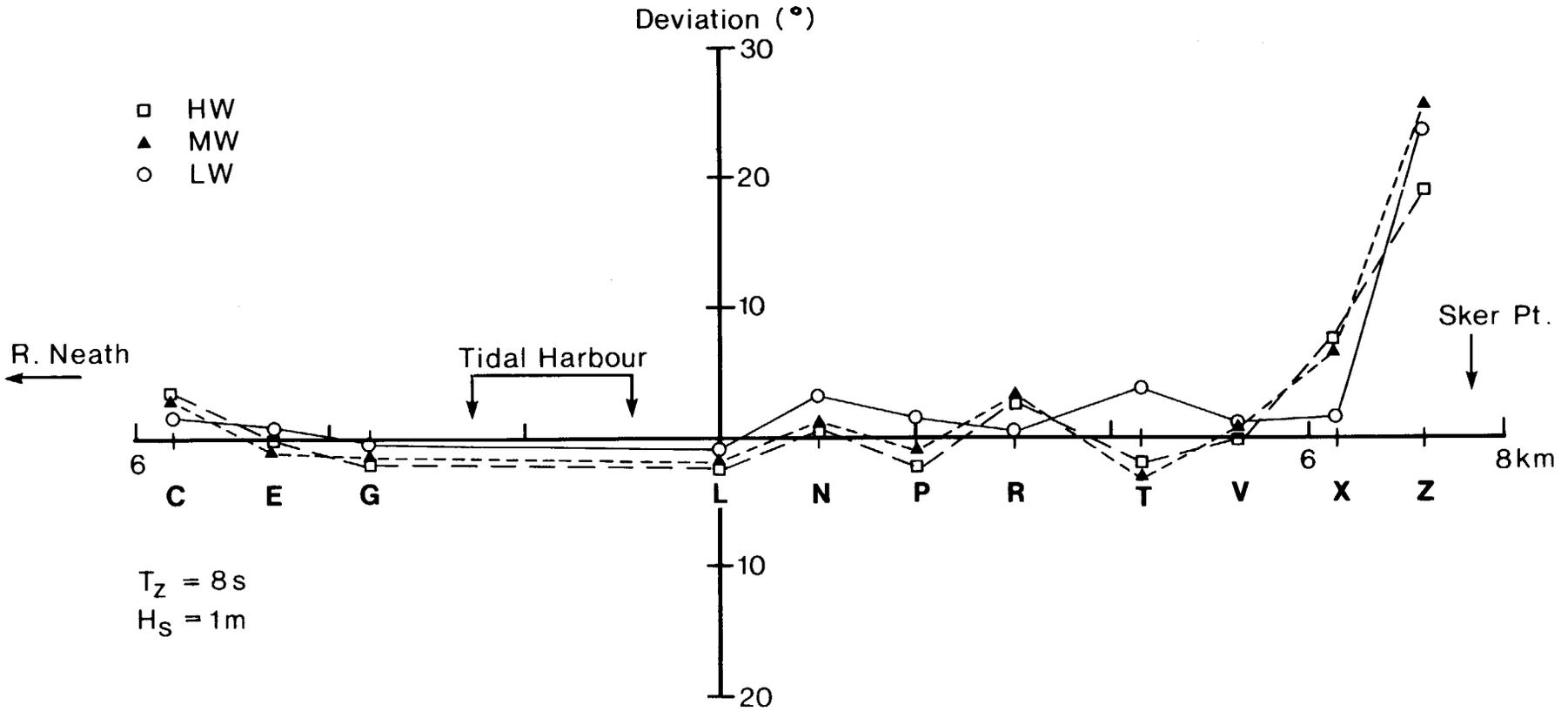

Figure 21 Deviations from normal wave incidence with respect to the alignment of the beach at the Low Water level for offshore wave approach directions between 220° and 270° and for water levels of 1.0, 5.25 and 9.50m above Chart Datum.

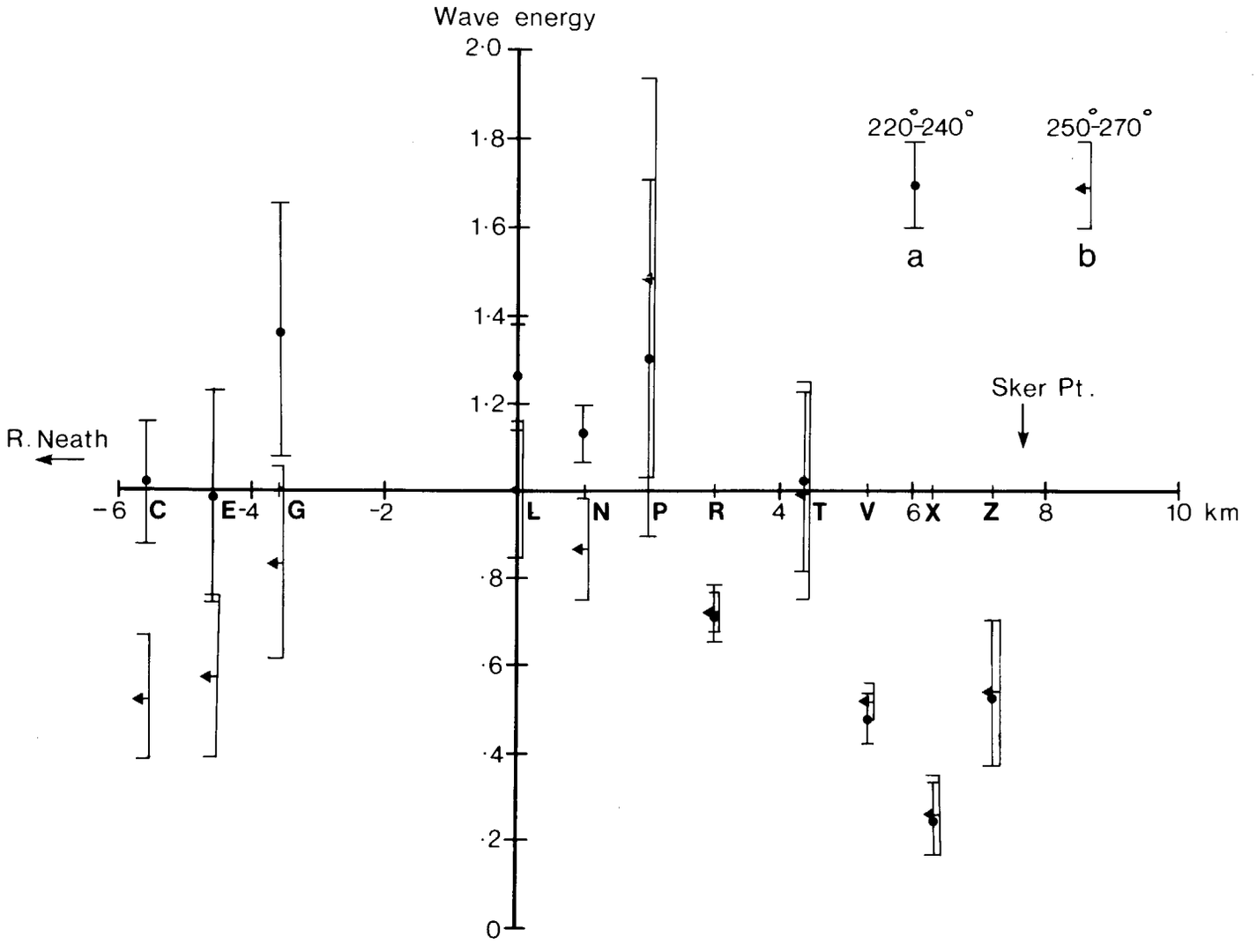

Figure 22 The alongshore variation of computed relative wave energy, normalised with respect to section L (250° - 270°), showing mean values, plus standard deviations, for offshore wave approach directions of (a) 220°, 230°, 240° and (b) 250°, 260°, 270° respectively, and for water levels of 1.0, 5.25, and 9.50m above CD. The wave height (H_s) was taken as 1m and wave period (T_z) as 8s.

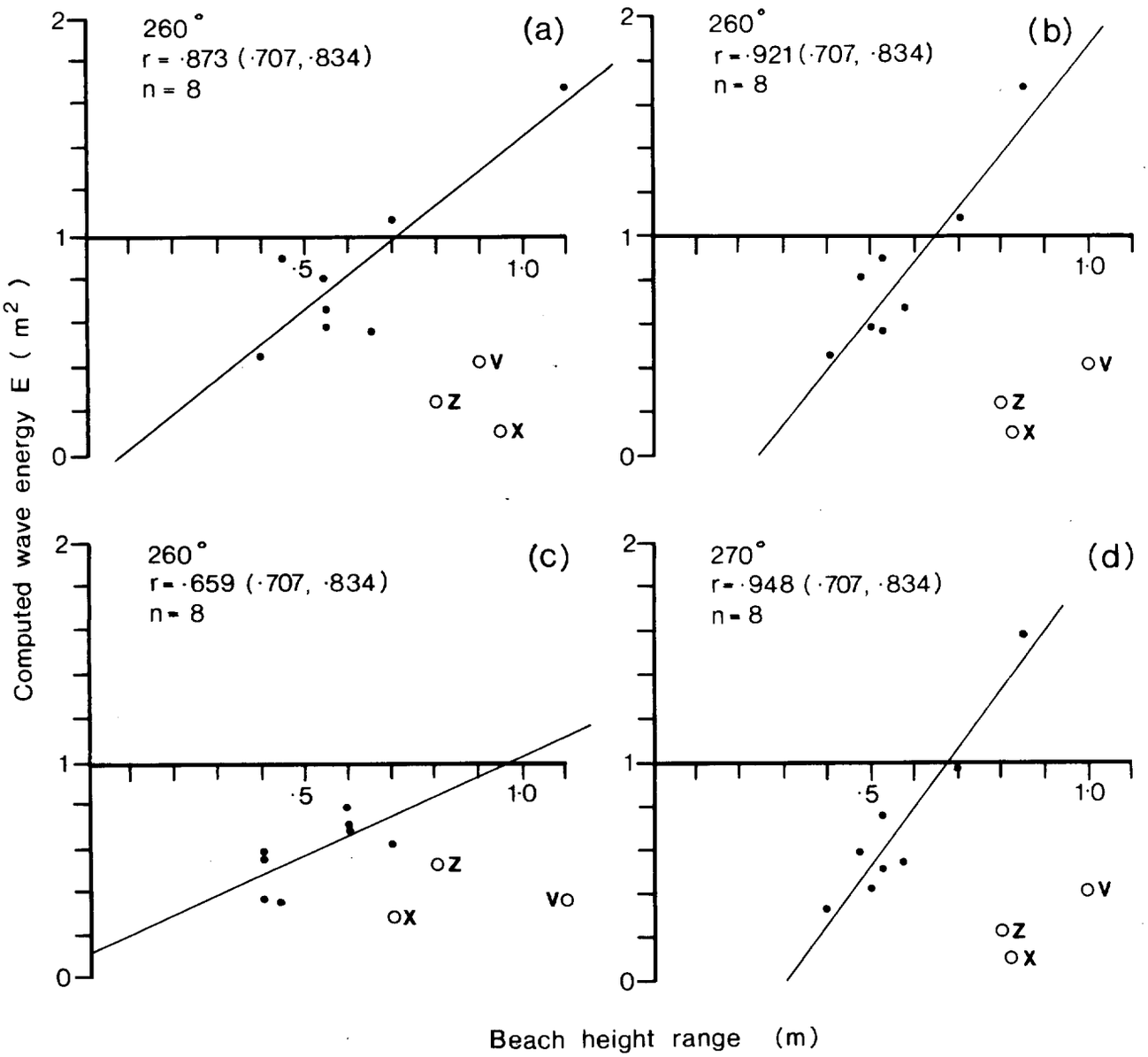

Figure 23 Relation of computed wave energy (E) to beach height variability for of shore wave approach directions of 260°(a,b,c) and 270°(d)and for a wa height (H_s) of 1m and a wave period (T_z) of 8s. This figure shows: (a) computed wave energy at the LW level (CD +1m) versus lower beach change; (b) computed wave energy at the HW level (CD +9.5m) versus upper beach change; (c) computed wave energy at the LW level (CD + 1m versus average beach change; (d) computed wave energy at the LW level (CD + 1m) versus average beach change. Points V, X and Z were omitted from the correlations. Correlation coefficients (r) are indicated together with their values at the 5% and 1% levels of significance (in brackets). n is the number of sections.

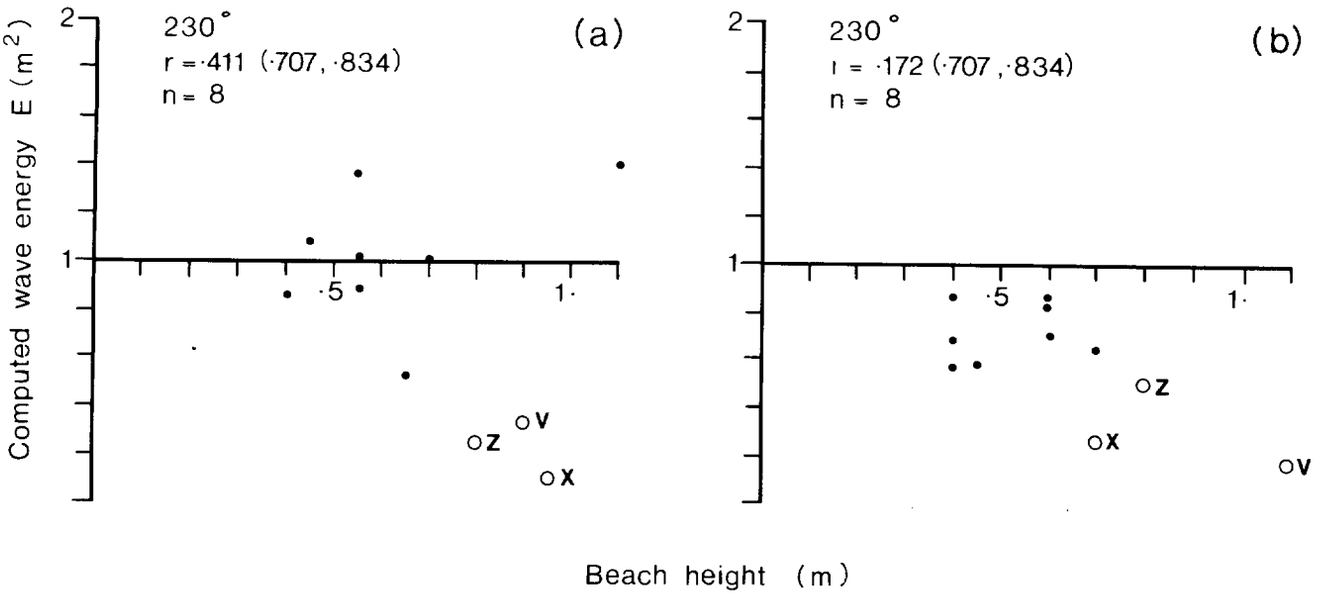

Figure 24 Relation of computed wave energy (E) to beach height variability for an offshore wave approach direction of 230° and for a wave height (H_s) of 1m and a wave period (T_z) of 8s. This figure shows (a) computed wave energy at the LW level (CD + 1m) versus lower beach change; (b) computed wave energy at the HW level (CD + 9.5m) versus upper beach change. Points V, X and Z were omitted from the correlations. Correlation coefficients (r) are shown together with their values at the 5% and 1% levels of significance (in brackets). n is the number of sections.

APPENDIX A

CALCULATION OF EFFECTIVE FETCH

Effective fetches given in Table 1 were calculated using the method given by CERC (1973).

Consider waves arriving at Point A in Figure A1. The wave height for a particular wind speed W blowing from the direction shown is some function of the sum of all the wind energy components acting along the radial fetches X_i, out to $\pm 45^\circ$ either side of the wind direction multiplied by the radial fetch. Thus -

$$\text{wave height at A} \propto \sum_{i=1}^{N} (W \cos \alpha_i)^2 X_i \ .$$

This wave height is equivalent to that which would be given by radial fetches X_i' ; corresponding to an effective geometric fetch in deep water of X_{eff} where

$$X_i' \cos \alpha_i = X_{eff} \ . \qquad \text{(A.1)}$$

Thus

$$\sum_{i=1}^{N} (W \cos \alpha_i)^2 X_i = \sum_{i=1}^{N} (W \cos \alpha_i)^2 X_i' \qquad \text{(A.2)}$$

which from equation (A.1) gives

$$X_{eff} = \frac{\Sigma X_i \cos^2 \alpha_i}{\Sigma \cos \alpha_i} \ . \qquad \text{(A.3)}$$

The values of X_{eff} shown in Table 1 were calculated using measured geometric fetches (X_i) and for angles out to 40°, in steps of 10°, on both sides of the assumed wind direction. Effective fetch bearings were taken in 10° intervals from 0° to 350°

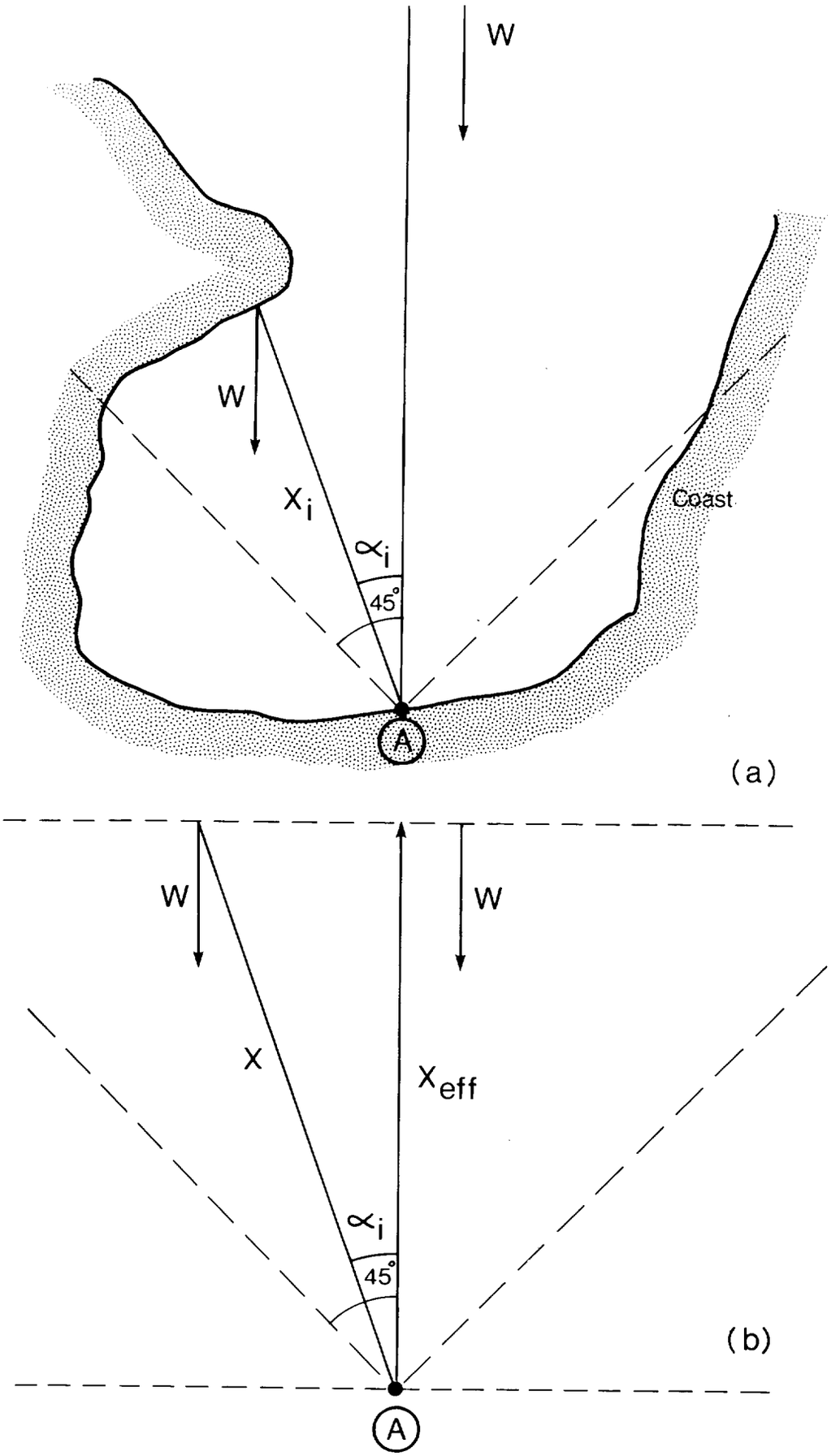

Figure A1

APPENDIX B

DETAILS OF WAVE REFRACTION CALCULATIONS

The following description of the wave refraction analysis program is taken from King and Hardcastle (1980). For full details see Abernethy and Gilbert (1974).

B.1 Ray Tracking

Linear wave theory gives the result that

$$\sigma c = g \tanh \frac{\sigma \lambda}{c} \qquad \text{(B.1)}$$

where σ is the angular frequency of the wave ,
c is the phase speed (or celerity) of the wave ,
λ is the water depth and
g is the acceleration due to gravity .

If the seabed is defined over a rectangular set of grid points and a diagonal drawn across each rectangle, the depths (λ) are defined in terms of a series of triangles, in which the celerity (c) may be interpolated using the formula

$$c = px + qy + r \qquad \text{(B.2)}$$

where p , q and r are constants. This formula is continuous across all triangle boundaries and furthermore by using the linear representation of c in equation (B.2) and Snell's Law (equation 6) it can be shown that the ray path through any triangle is an arc of a circle. Thus given a wave frequency and initial direction, a wave ray may be tracked from any starting point within the grid area, triangle by triangle, until it reaches an end point.

B.2 Energy Transfer Functions

Let the directional wave spectrum be defined by $S(f, \theta)$ where f is frequency and θ is direction. It can be shown (Longuet-Higgins, 1957) that, by making certain assumptions, $S(k_1, k_2)$ is constant along a wave ray path, where $\underline{k} = (k_1, k_2)$ is a two dimensional (vector) wave number. Transforming from wave number space to frequency and direction space to maintain volume elements of energy gives

$$S(f,\theta)\,df\,d\theta = S(k_1,k_2)\,dk_1\,dk_2 \qquad \text{(B. 3)}$$

whence

$$S(k_1,k_2) = S(f,\theta)\frac{df}{dk_1}\cdot\frac{d\theta}{dk_2} \qquad \text{(B.4)}$$

which since $dk_1\,dk_2 = k\,dk\,d\theta$, where $k = |\underline{k}|$ gives,

$$S(k_1,k_2) = S(f,\theta)\frac{1}{k}\cdot\frac{df}{dk}\,. \qquad \text{(B.5)}$$

Since the group velocity of waves is by definition

$$c_g = \frac{d\omega}{dk} \qquad \text{(B.6)}$$

where $\omega = 2\pi f$ and since $k = c/2\pi f$ then equation (B.5) becomes

$$S(k_1,k_2) = \frac{c\,c_g}{f}\cdot S(f,\theta) = \text{constant}\,. \qquad \text{(B.7)}$$

Thus from Longuet-Higgins (1957) $c\,c_g\,S(f,\theta)$ is constant along a ray path whenever f is constant. Therefore by defining $S_i(f,\theta_i)$ and $S_o(f,\theta_o)$ as the inshore and offshore spectra then from (B.7)

$$(c\,c_g)_i\;S_i(f,\theta_i) = (c\,c_g)_o\;S_o(f,\theta_o) \qquad \text{(B.8)}$$

or

$$S_i(f,\theta_i) = \mu(f)\,S_o(f,\theta_o) \qquad \text{(B.9)}$$

where

$$\mu(f) = \frac{(c\,c_g)_o}{(c\,c_g)_i}\,. \qquad \text{(B.10)}$$

To obtain inshore values for H_s and T_z, $S_i(f)$ is required where

$$S_i(f) = \int_{\theta_{i_1}}^{\theta_{i_2}} S_i(f,\theta_i)\,d\theta_i \qquad \text{(B.11)}$$

$$= \mu(f)\int_{\theta_{i_1}}^{\theta_{i_2}} S_o(f,\theta_o)\,d\theta_i \qquad \text{(B.12)}$$

where θ_{i_1} to θ_{i_2} is the range of interest at the target point. Assuming that $S_o(f, \theta_o)$ is sufficiently smooth then

$$S_o(f, \theta_o) = \sum_{n=1}^{N} \frac{A_n(f)}{\Delta_o \theta} \quad H(\theta - n\Delta_o\theta) \qquad \text{(B.13)}$$

where

$\Delta_o\theta$ is the angular segment of the offshore direction,
N is the number of segments,
$A_n(f)$ is the total energy at frequency f in directional segment n (ie $n\Delta_o\theta \leq \theta_o \leq (n+1)\Delta_o\theta$),
$H(x)$ = 1 if $0 < x \leq \Delta_o\theta$,
= 0 otherwise.

Substituting for $S_o(f, \theta_o)$ in the expression for $S_i(f)$ and approximating the integral by a summation over the number of rays arriving at the inshore target point(ray paths are reversed after tracking) gives

$$S_i(f) = \mu(f) \frac{\Delta_i\theta}{\Delta_o\theta} \sum_{n=1} N_n A_n(f) = \sum_n A_n T_n \qquad \text{(B.14)}$$

where

$$T_n(f) = \mu(f) N_n \frac{\Delta_i\theta}{\Delta_o\theta} \qquad \text{(B.15)}$$

and $\Delta_i\theta$ is the angle between rays arriving at the target-point and N_n is the number of rays whose offshore direction θ_o is in the nth directional segment.

The inshore H_s and T_z values can be calculated from the zero and second order moments of $S(f)$ (Cartwright and Longuet-Higgins, 1956). That is

$$H_s = 4M_o^{1/2} \quad \text{and} \quad T_z = 2\pi(M_o/M_2)^{1/2} \qquad \text{(B.16)}$$

where

$$M_o = \int_0^\infty S(f)\,df \quad \text{and} \quad M_2 = 4\pi^2 \int_0^\infty f^2 S(f)\,df. \qquad \text{(B.17)}$$

For the computations the integrals are replaced by summations, assuming Δf is sufficiently small. To obtain an estimate of the mean inshore

wave direction $\bar{\theta}(f)$, the series approximation (B.13) for is substituted in the definition of the mean vector at the target point, namely

$$\overline{V} = \frac{\int_{\theta_{i_1}}^{\theta_{i_2}} S_i(f,\theta_i)\, e^{i\theta_i}\, d\theta_i}{\int_{\theta_{i_1}}^{\theta_{i_2}} S_i(f,\theta_i)\, d\theta_i} \quad . \tag{B.18}$$

Thus

$$\bar{\theta}(f) = \tan^{-1} \sum_n A_n(f)\, V_n(f) \Big/ \sum_n A_n(f)\, U_n(f) \tag{B.19}$$

where

$$U_n(f) + i\, V_n(f) = \mu(f) \frac{\Delta_i\theta}{\Delta_0\theta} \sum_{\substack{\text{rays in} \\ \text{segment} \\ n}} e^{i\theta_i} \quad . \tag{B.20}$$

Thus the transfer functions (see Section 3.2) T_n, U_n, V_n are calculated from

$$\begin{pmatrix} T_n \\ U_n \\ V_n \end{pmatrix}(f) = \mu(f) \frac{\Delta_i\theta}{\Delta_0\theta} \sum_{\substack{\text{rays in} \\ \text{segment} \\ n}} \begin{pmatrix} 1 \\ \cos\theta_i \\ \sin\theta_i \end{pmatrix} \tag{B.21}$$

for the set of frequencies $\{f_m : m = 1, \ldots\ldots M\}$ and stored in a file as the matrix elements $T_{nm} = T_n(f_m)$, $U_{nm} = U_n(f_m)$ and $V_{nm} = V_n(f_m)$. Once these functions are available it is a relatively fast calculation to determine $S_i(f_m)$ and $\bar{\theta}(f_m)$ from equations (B.14) and (B.19) and from the offshore spectral matrix $\{A_{nm} = A_n(f_m)\}$.

B.3 Offshore wave spectrum forms

The offshore values $\{A_{nm}\}$ can be estimated in a variety of ways. Since it is usually the frequency spectrum $S(f)$ that is studied rather than $S(f,\theta)$, the directional distribution is assumed. Thus

$$S_0(f,\theta) = S_0(f)\, G(\theta) \tag{B.22}$$

where

$$G(\theta) = \frac{2}{\pi} \cdot \cos^2(\theta - \theta_m) \tag{B.23}$$

for $|\theta - \theta_m| \leq \pi/2$ and where θ_m is the mean direction (Hasselman, 1973).

Values of $S_0(f)$ can either be taken directly from a frequency spectral analysis of the offshore wave data, or can be estimated using a theoretical (empirical) approximation (eg Pierson-Moskowitz).

Since the available offshore wave data was mostly in the form of H_s and T_z values, the approximation used for this comparison was one derived from the Pierson-Moskowitz spectrum to include the parameters H_s and T_z. Thus

$$S_0(f) = \frac{H_s^2}{4\pi T_z^4 f^5} \cdot e^{-\frac{1}{\pi(T_z f)^4}} \qquad \text{(B.24)}$$

Thus values of $\{A_{nm}\}$ were calculated from the approximation

$$A_{nm} = A_n(f_m) = S_0(f_m) \cdot G(\theta_n) \cdot \Delta_0\theta \qquad \text{(B.25)}$$

where θ_n is the direction representative of the n th offshore directional segment.

APPENDIX C

WAVE REFRACTION DIAGRAMS

	Water depth (m)	Wave period (s)	Wave direction (^{o}T)
Figure C1	CD + 5.25	8	220
C2	CD + 5.25	8	230
C3	CD + 5.25	8	240
C4	CD + 5.25	8	250
C5	CD + 5.25	8	260
C6	CD + 5.25	8	270
C7	CD + 5.25	6	260
C8	CD + 5.25	10	260
C9	CD + 1.00	8	260
C10	CD + 9.50	8	260
C11	CD + 5.25	6	150
C12	CD + 5.25	6	160
C13	CD + 5.25	6	170
C14	CD + 5.25	4	160
C15	CD + 5.25	8	160

M = Mumbles

S = Swansea

PT = Port Talbot

SWANSEA BAY

WATER DEPTH CD+5.25M
WAVE PERIOD 8.S
WAVE DIRECTION 220.DEG

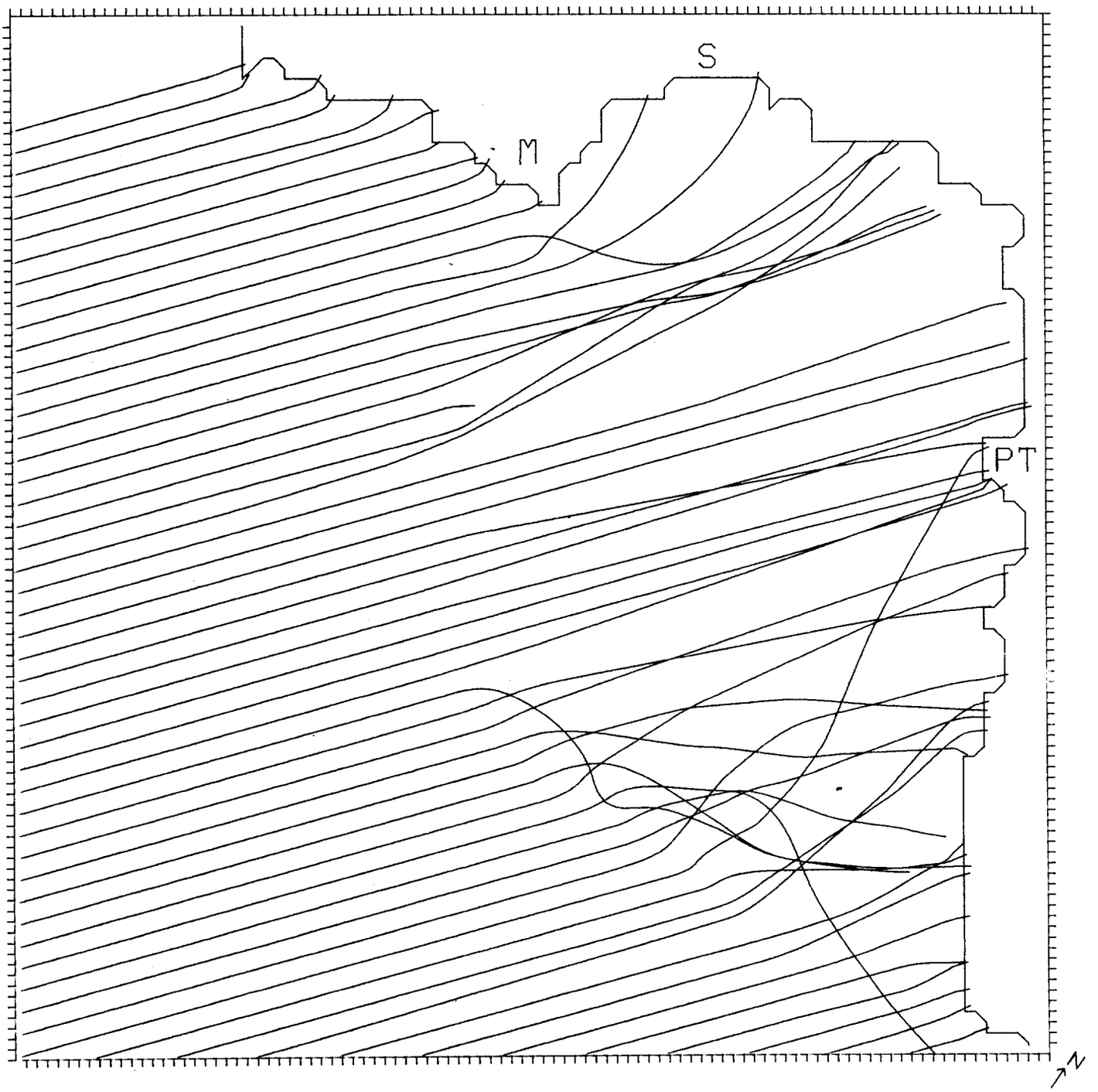

Figure C1

SWANSEA BAY

WATER DEPTH CD+5.25M

WAVE PERIOD 8.S

WAVE DIRECTION 230.DEG

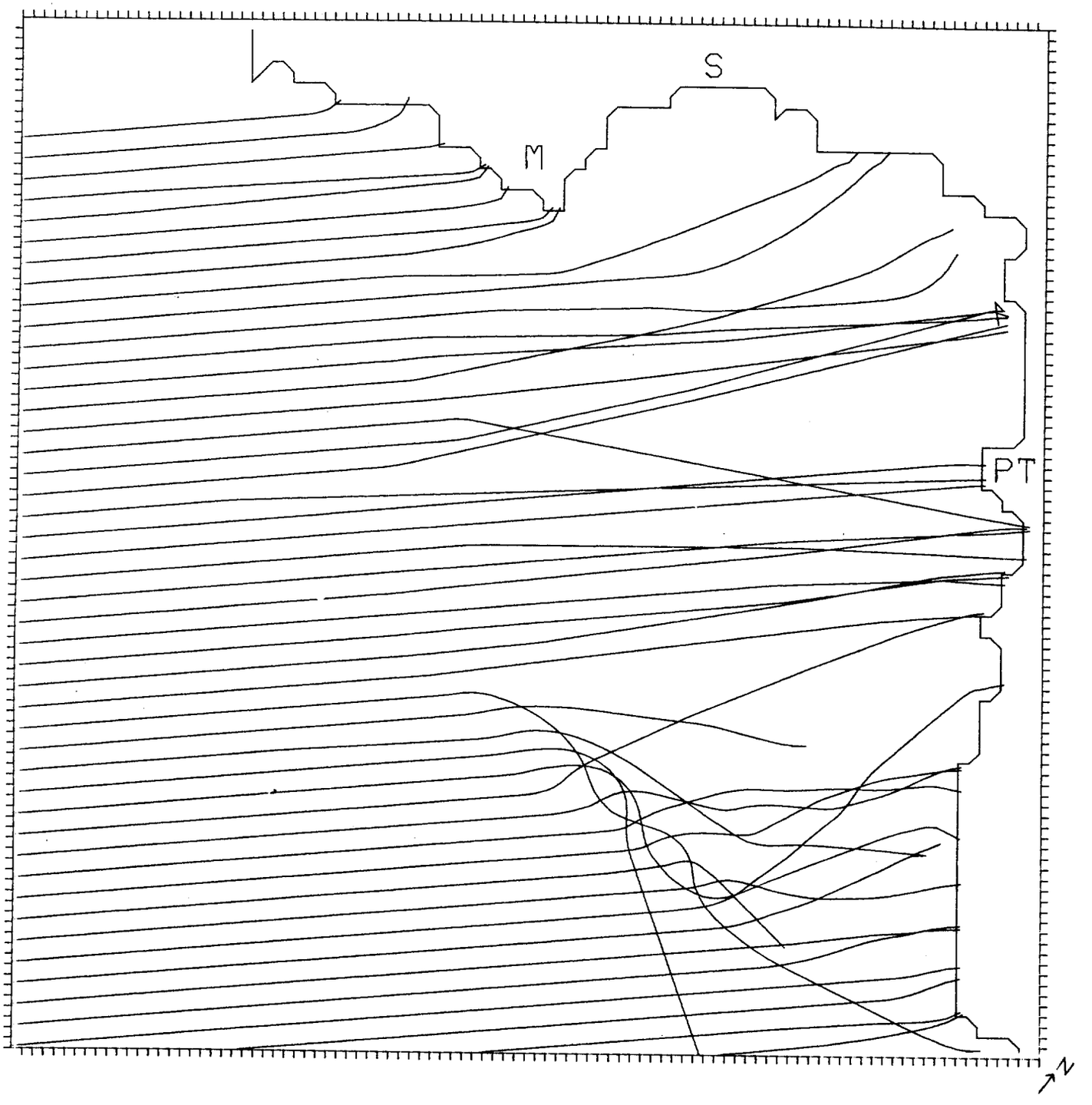

Figure C2

SWANSEA BAY

WATER DEPTH CD+5.25M

WAVE PERIOD 8.S

WAVE DIRECTION 240.DEG

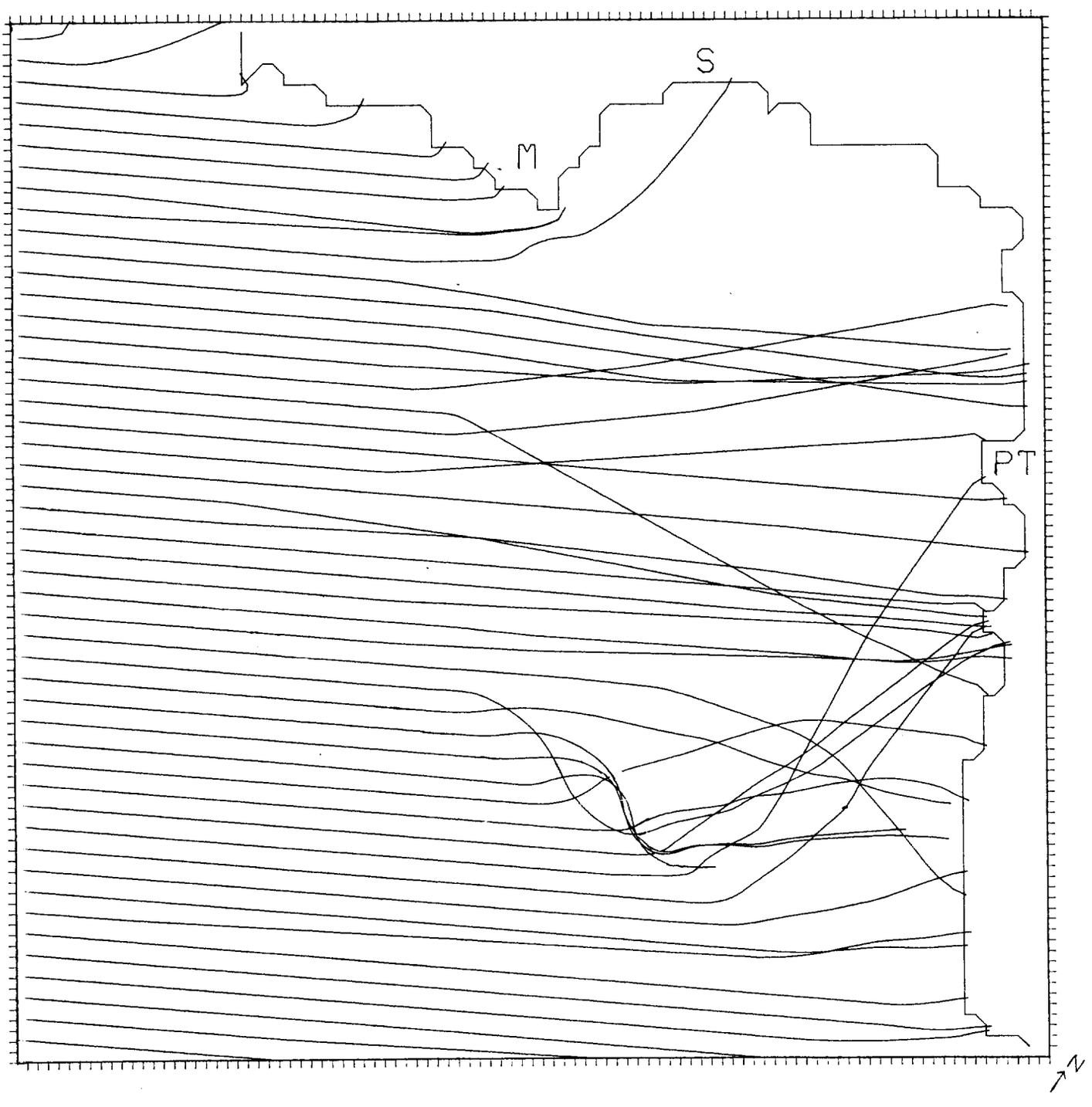

Figure C3

SWANSEA BAY

WATER DEPTH CD+5.25M
WAVE PERIOD 8.S
WAVE DIRECTION 250.DEG

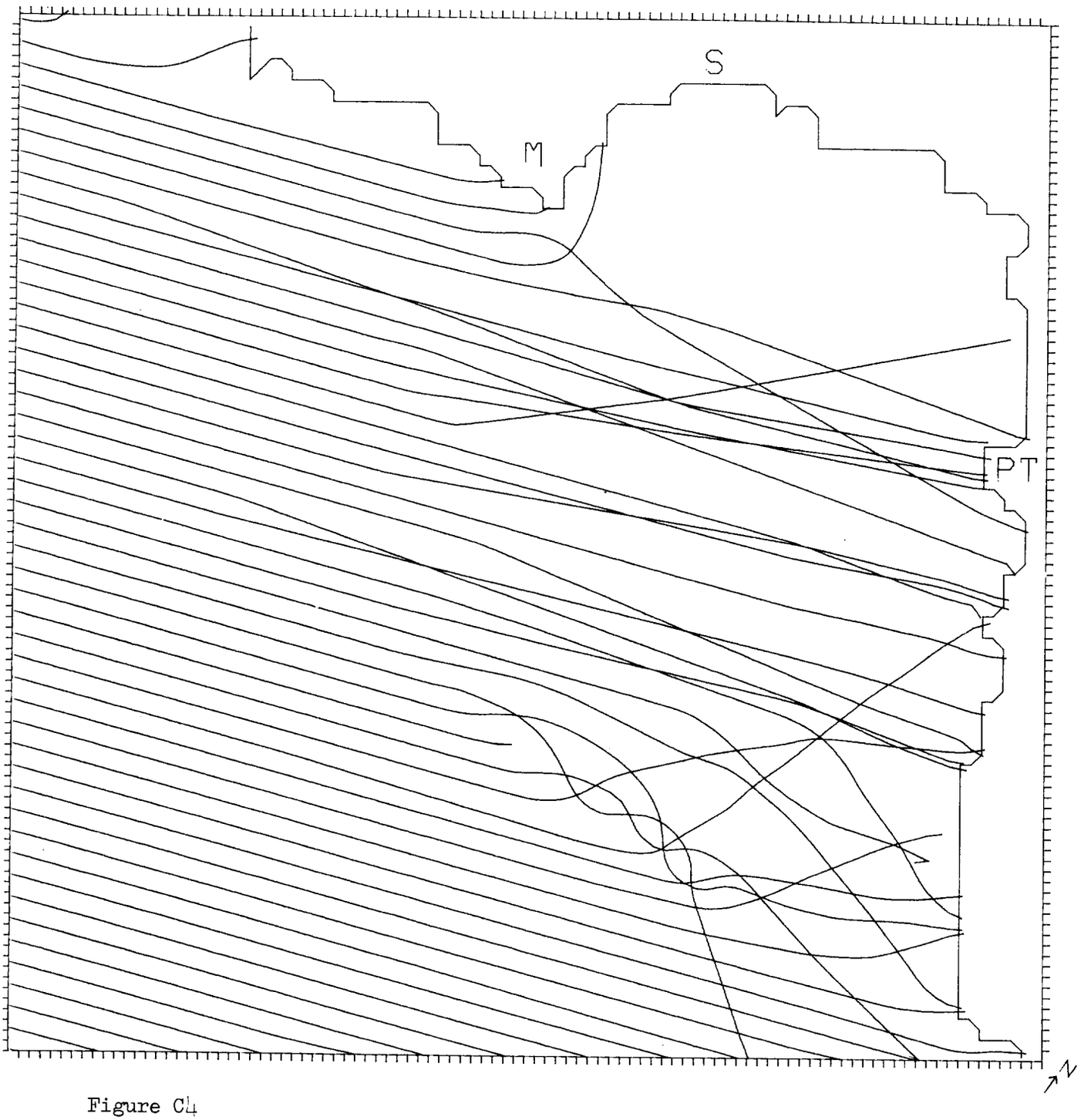

Figure C4

SWANSEA BAY

WATER DEPTH CD+5.25M
WAVE PERIOD 8.S
WAVE DIRECTION 260.DEG

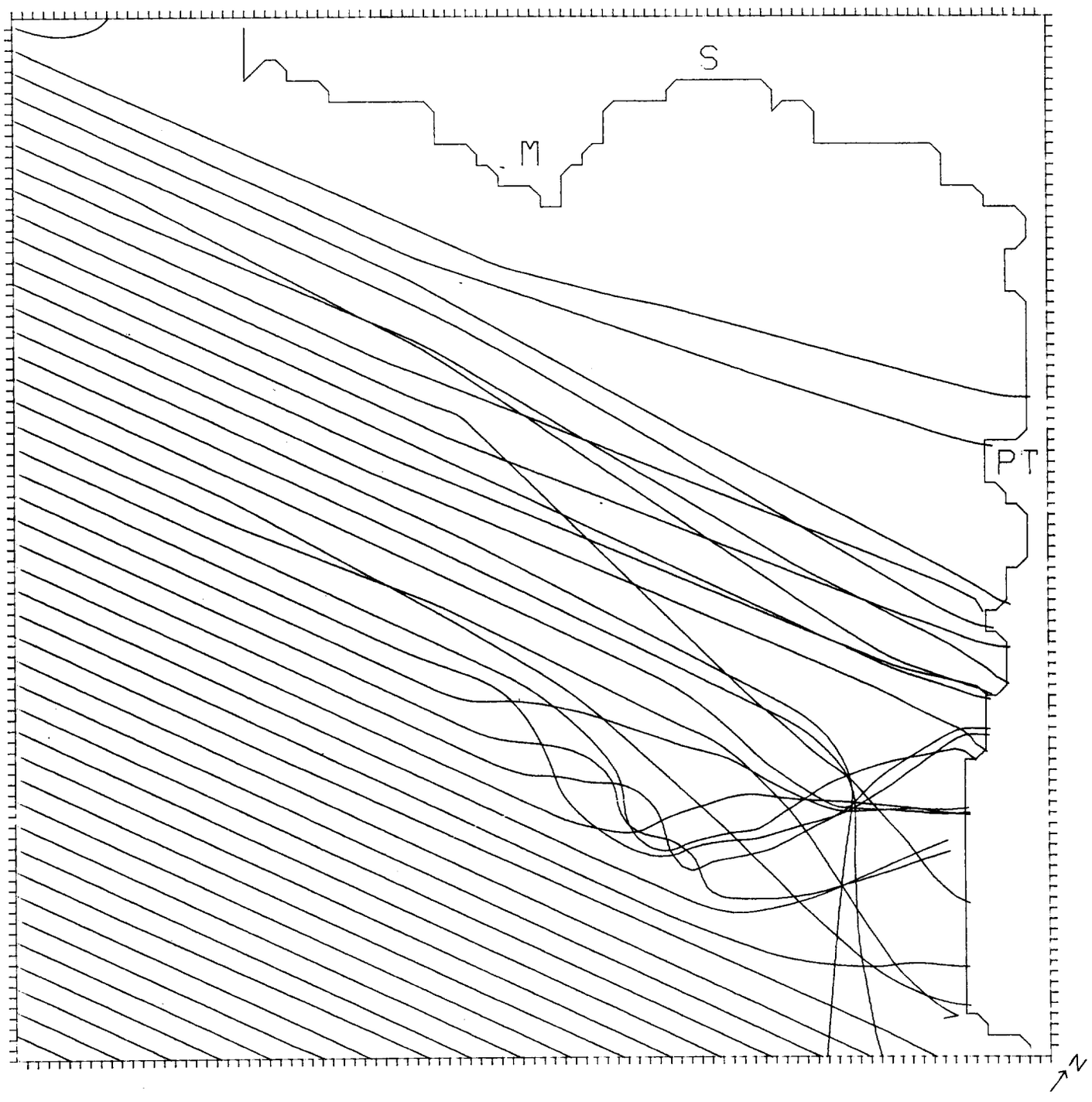

Figure C5

SWANSEA BAY

WATER DEPTH CD+5.25M
WAVE PERIOD 8.S
WAVE DIRECTION 270.DEG

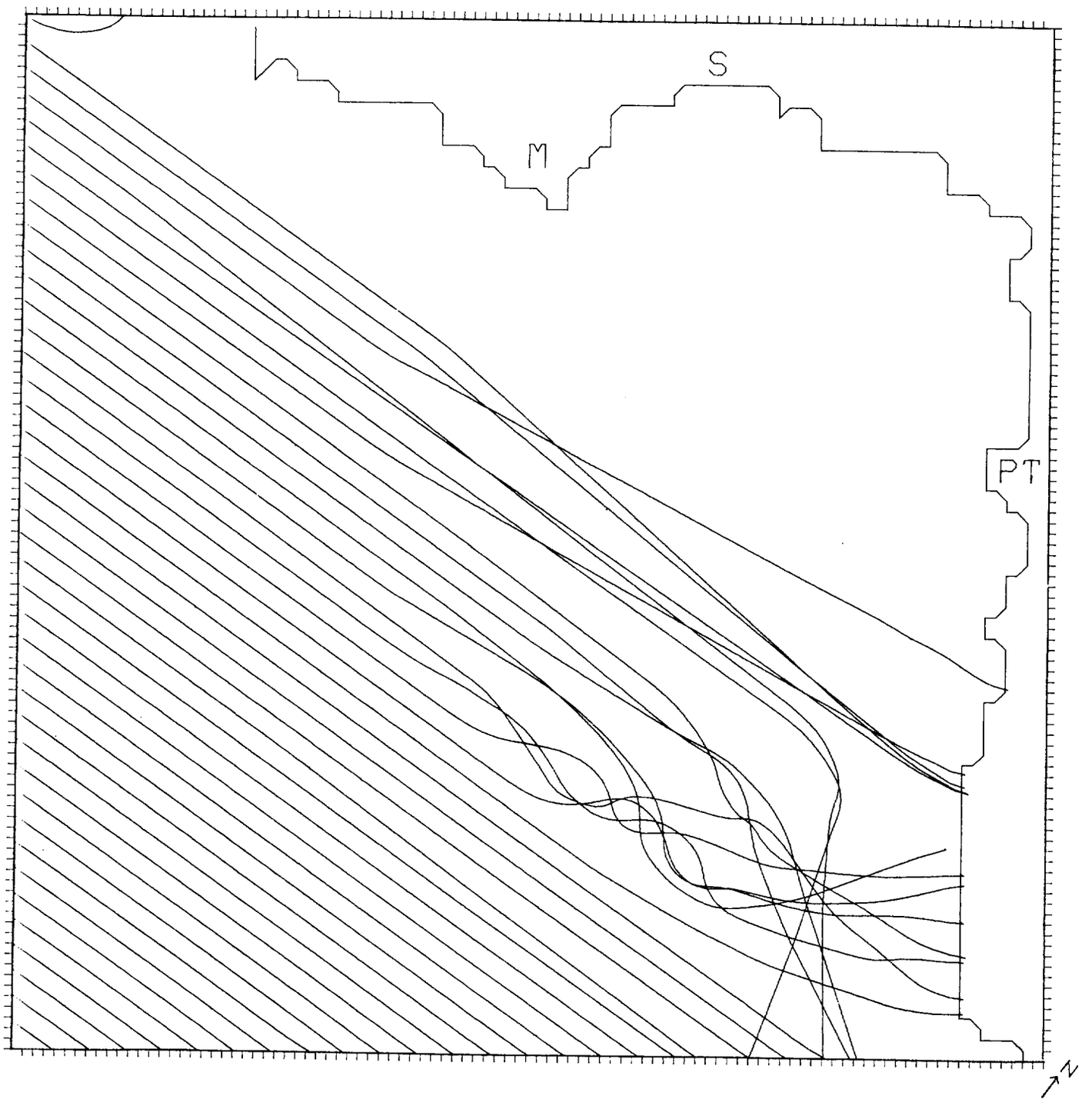

Figure C6

SWANSEA BAY

WATER DEPTH CD+5.25M
WAVE PERIOD 6.5
WAVE DIRECTION 260.DEG

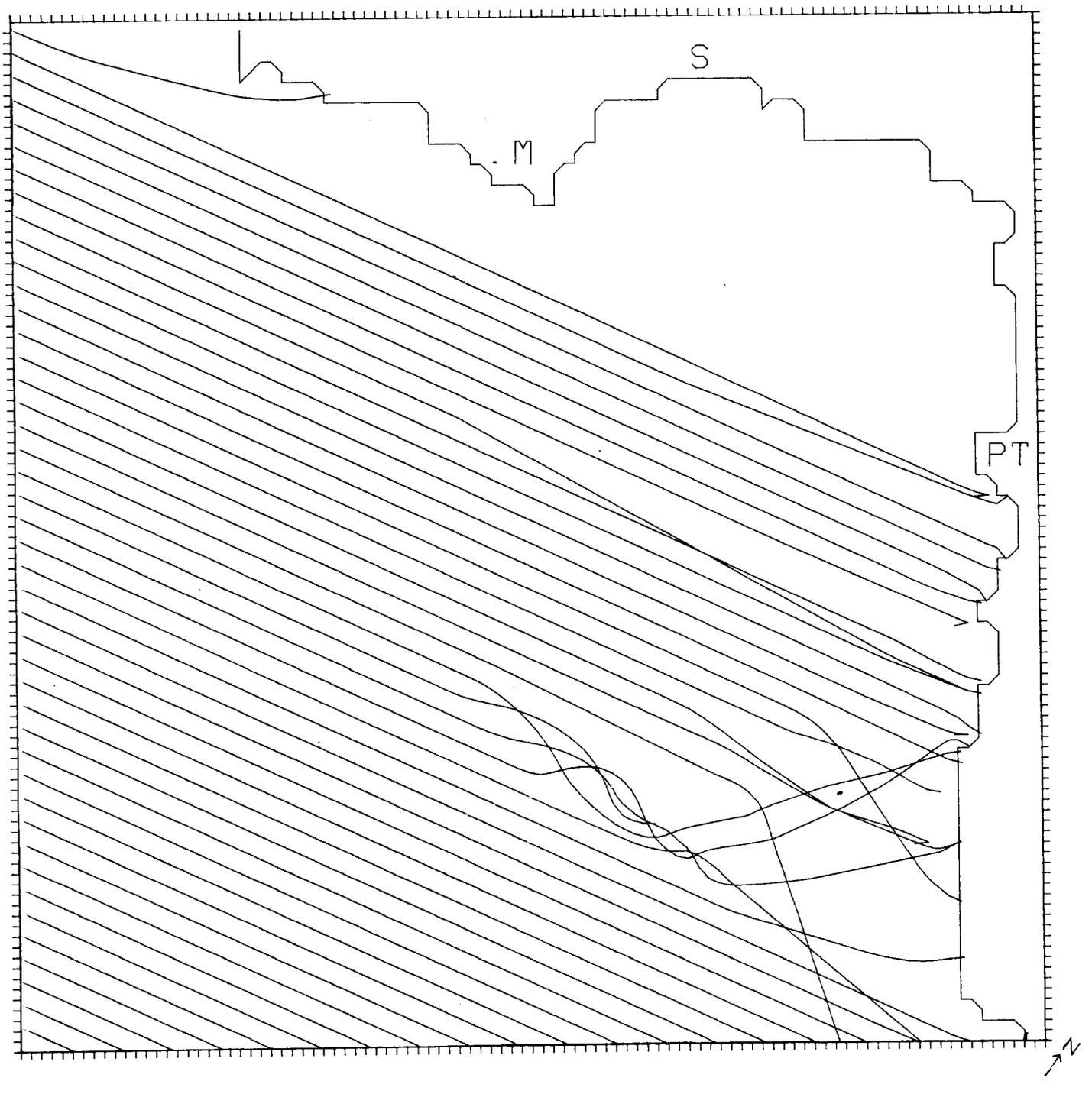

Figure C7

SWANSEA BAY

WATER DEPTH CD+5.25M
WAVE PERIOD 10.S
WAVE DIRECTION 260.DEG

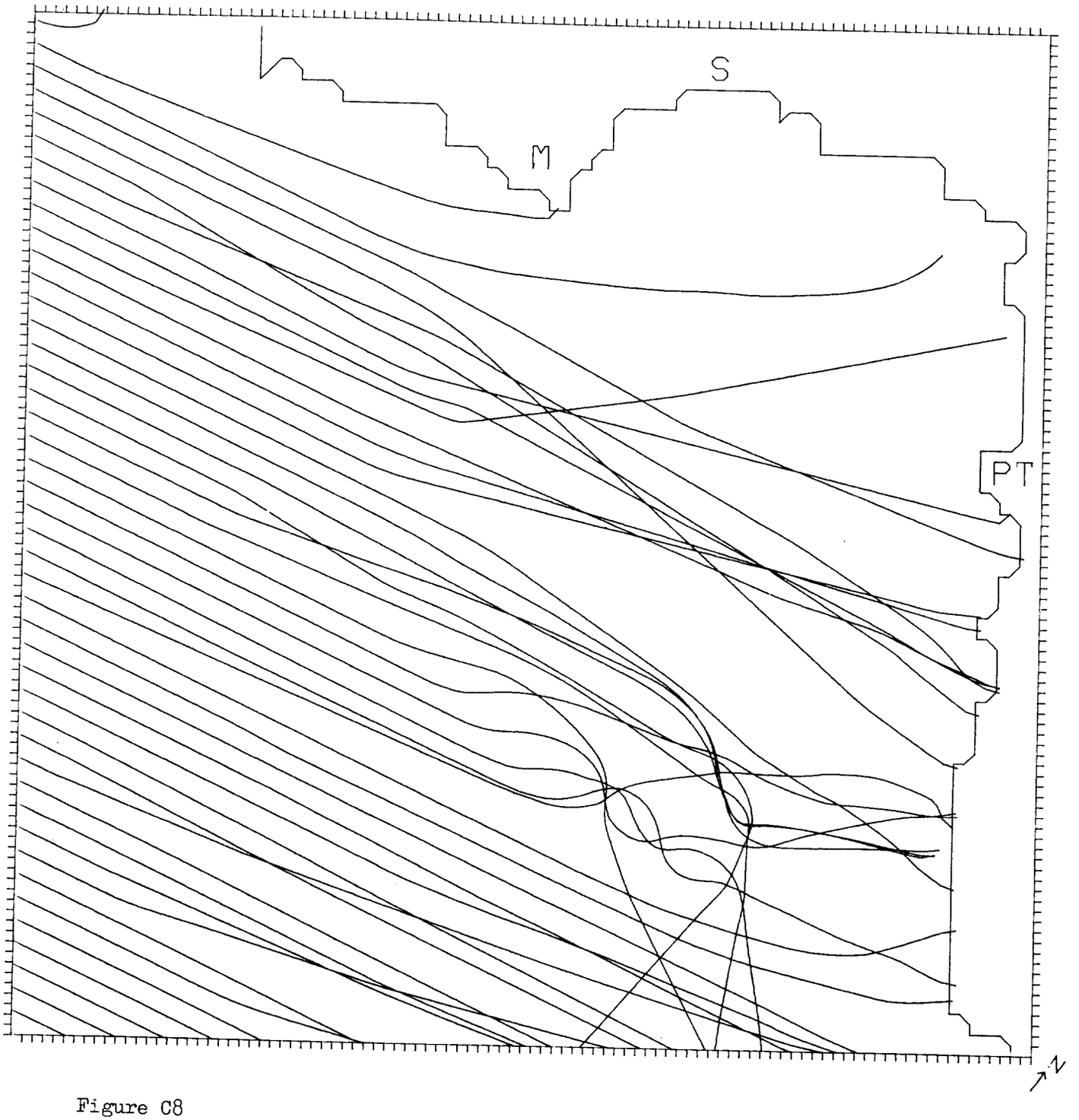

Figure C8

SWANSEA BAY

WATER DEPTH CD+ 1.M
WAVE PERIOD 8.S
WAVE DIRECTION 260.DEG

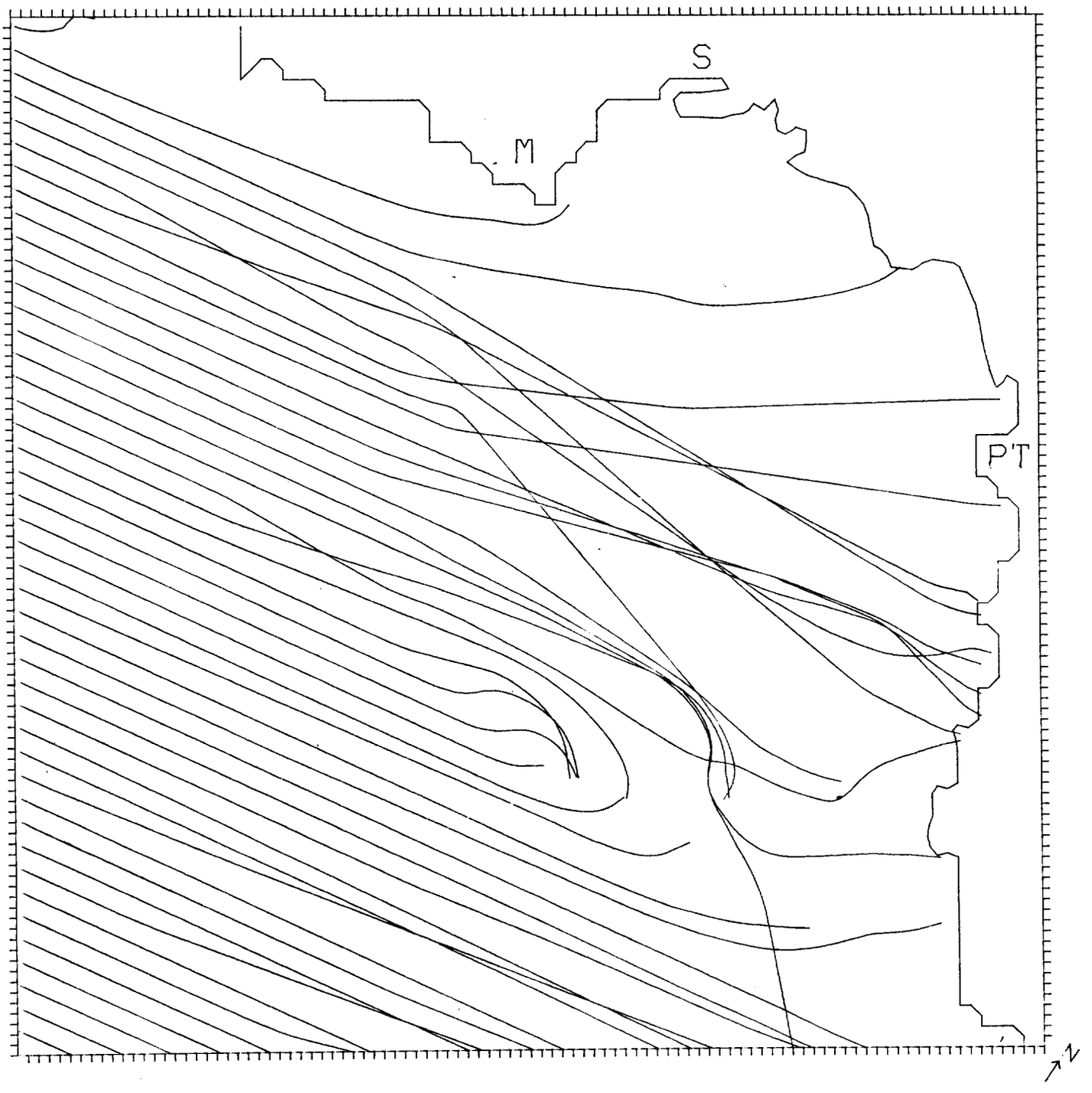

Figure C9

SWANSEA BAY

WATER DEPTH CD+ 9.5M
WAVE PERIOD 8.S
WAVE DIRECTION 260.DEG

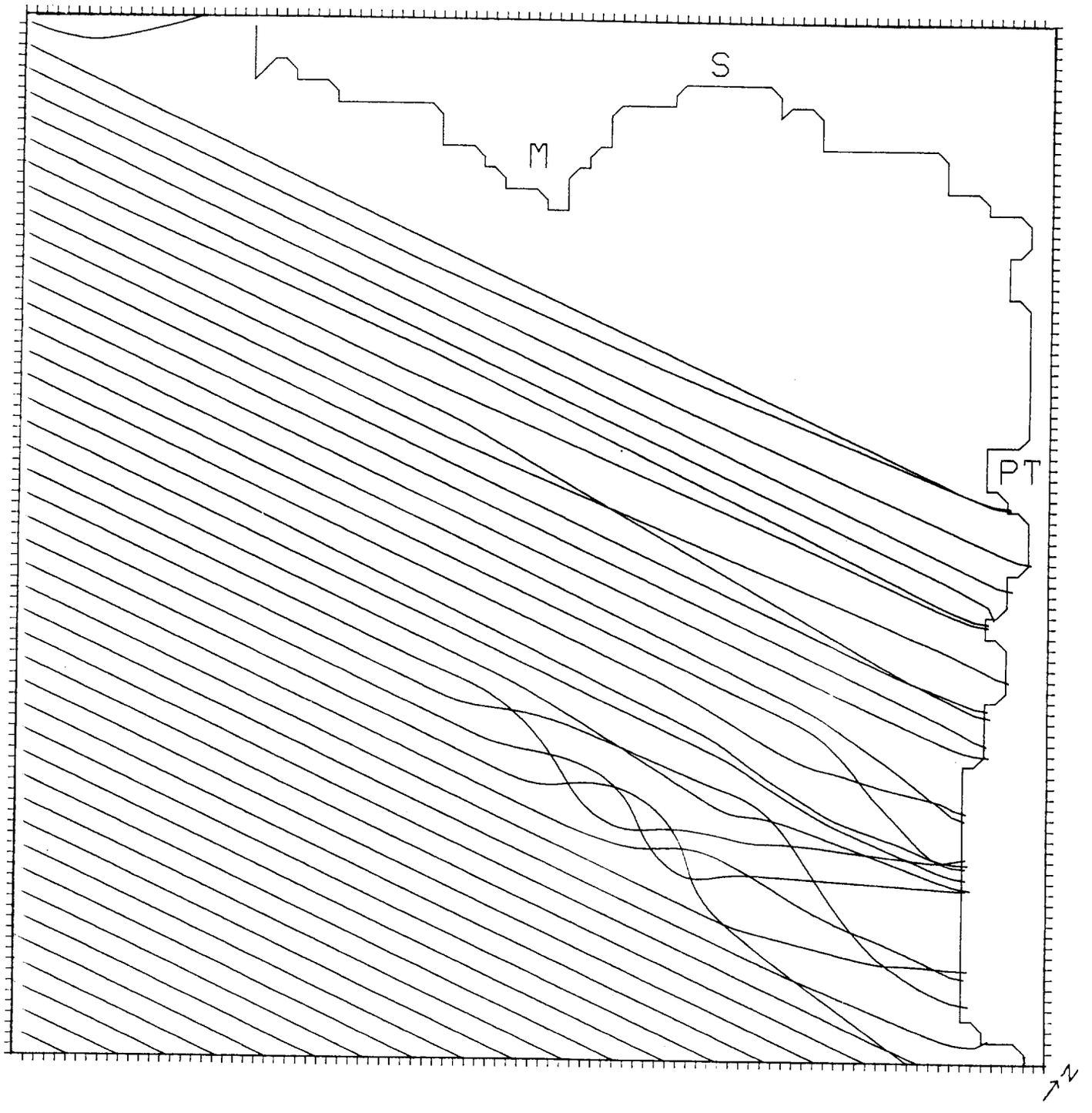

Figure C10

SWANSEA BAY

WATER DEPTH CD+5.25M
WAVE PERIOD 6.S
WAVE DIRECTION 150.DEG

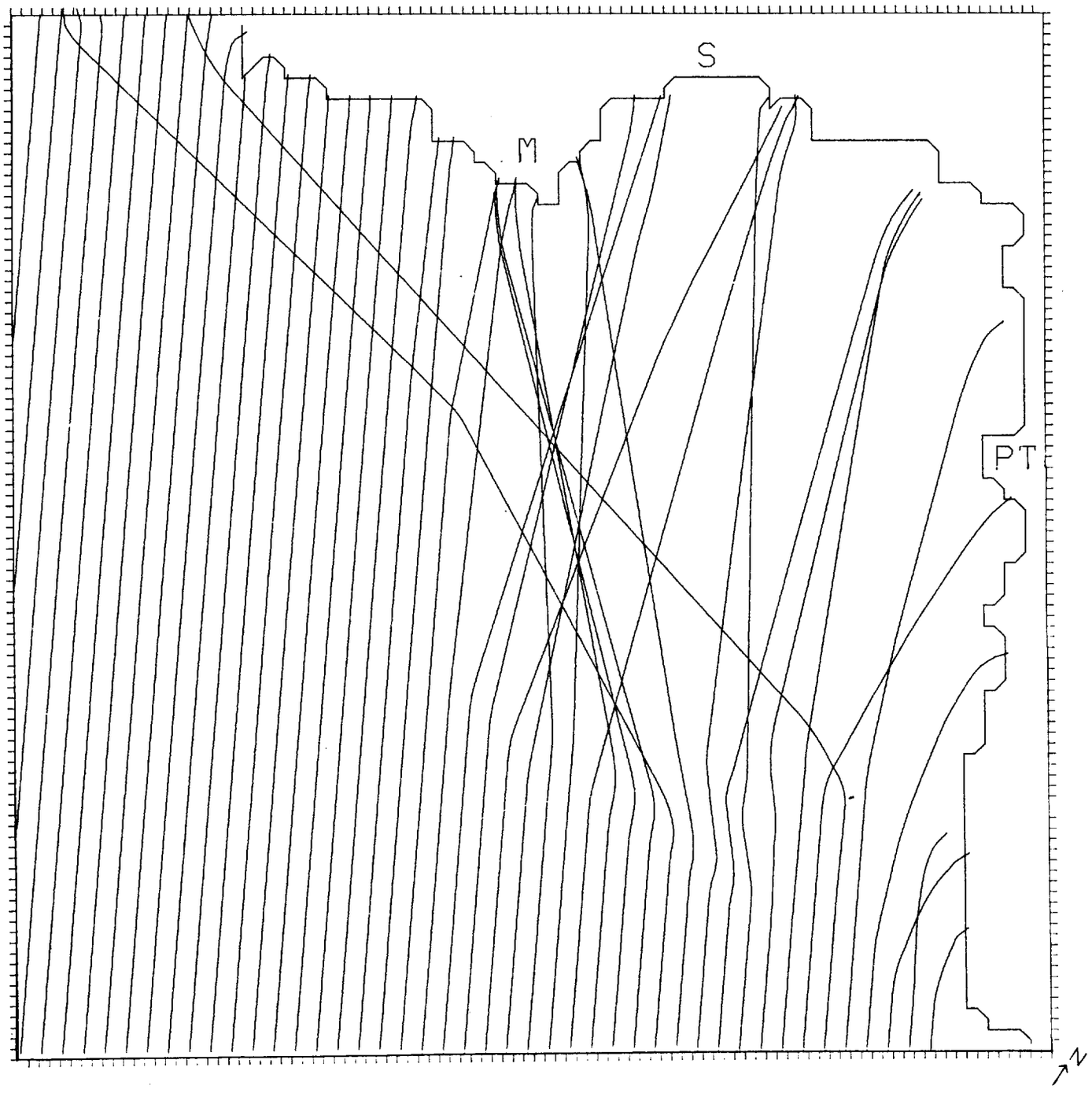

Figure C11

SWANSEA BAY

WATER DEPTH CD+5.25M
WAVE PERIOD 6.5
WAVE DIRECTION 160.DEG

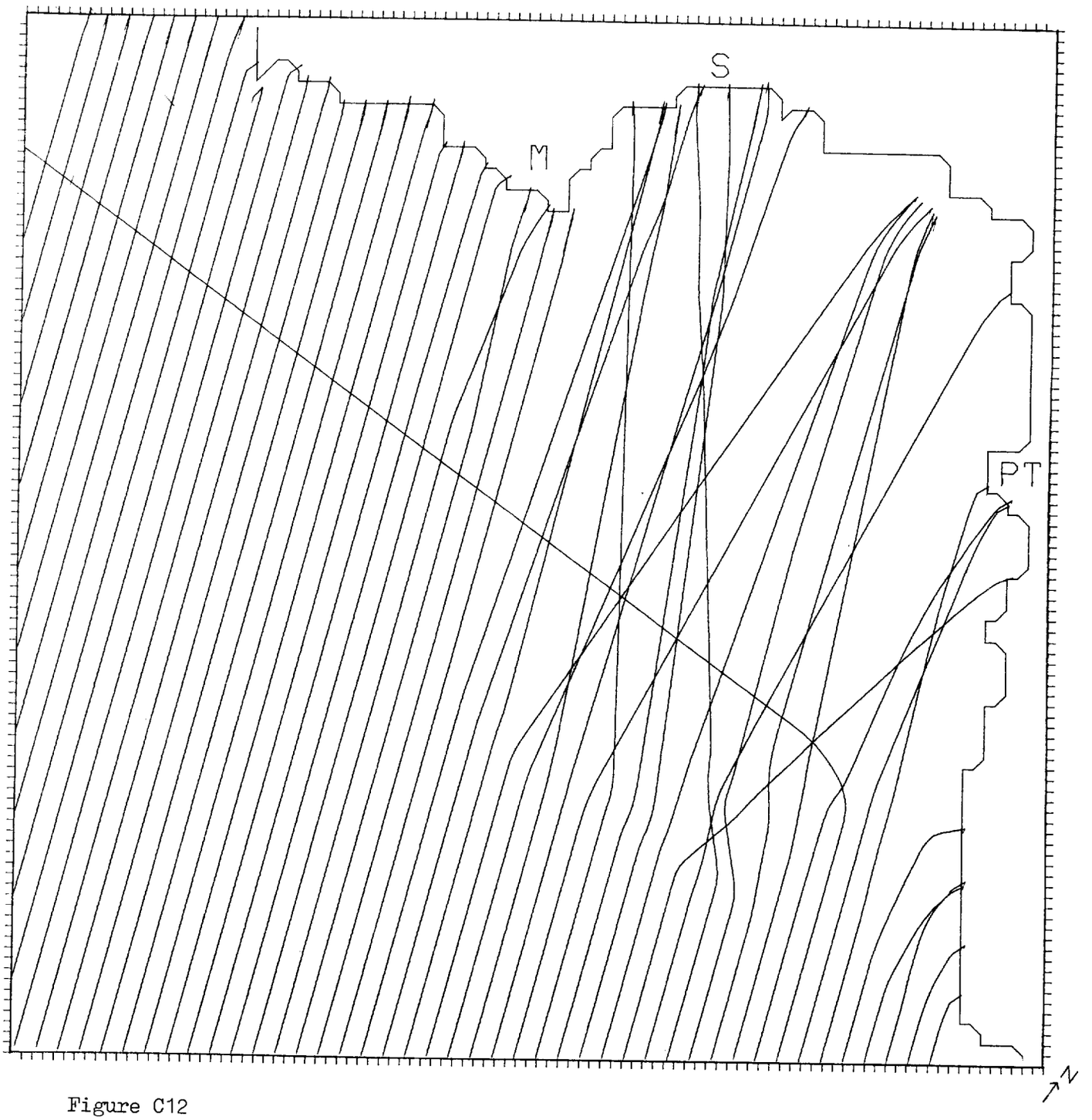

Figure C12

SWANSEA BAY

WATER DEPTH CD+5.25M
WAVE PERIOD 6.S
WAVE DIRECTION 170.DEG

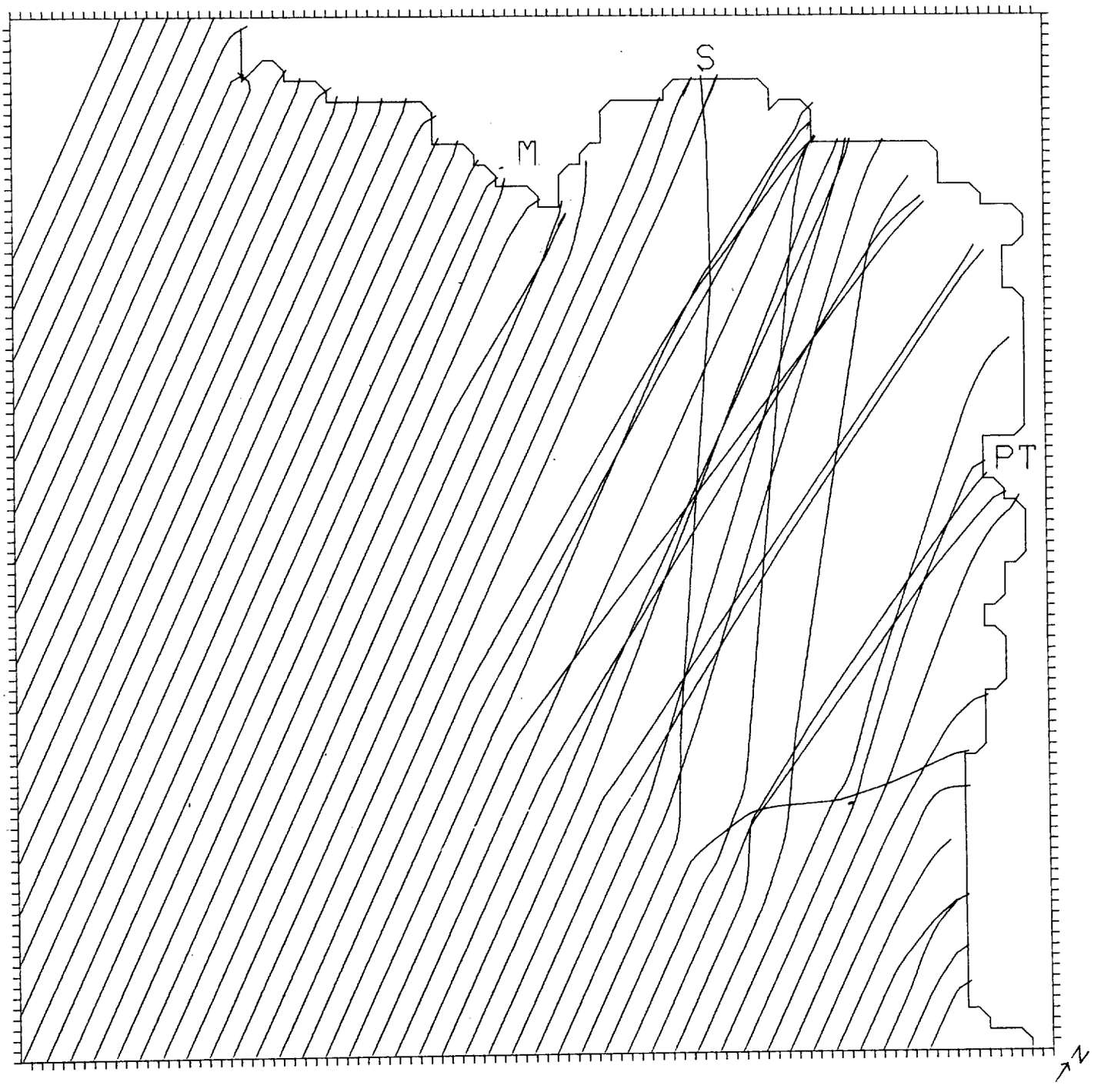

Figure C13

SWANSEA BAY

WATER DEPTH CD+5.25M

WAVE PERIOD 4.S

WAVE DIRECTION 160.DEG

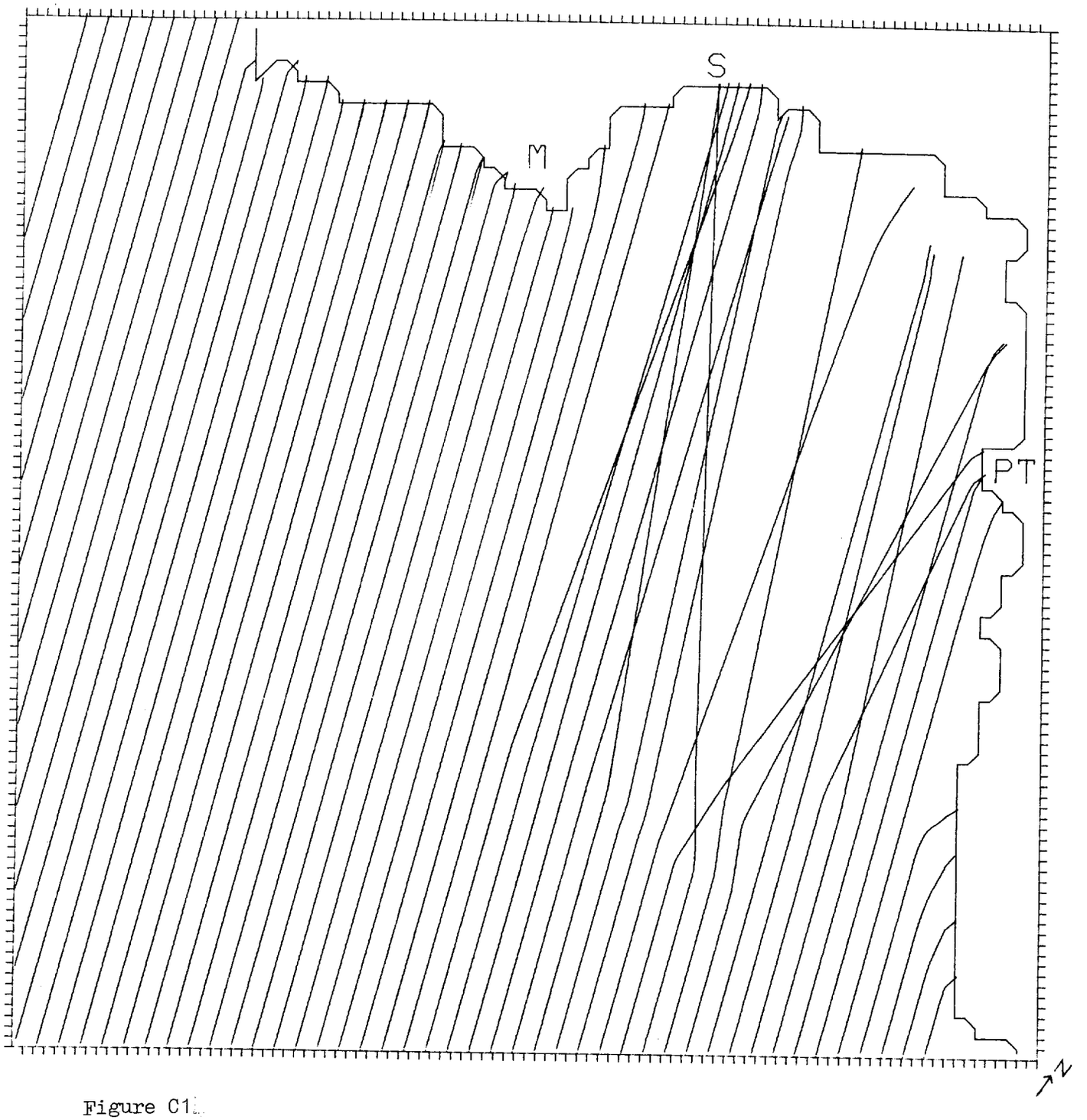

Figure C1

SWANSEA BAY

WATER DEPTH CD+5.25M
WAVE PERIOD 8.S
WAVE DIRECTION 160.DEG

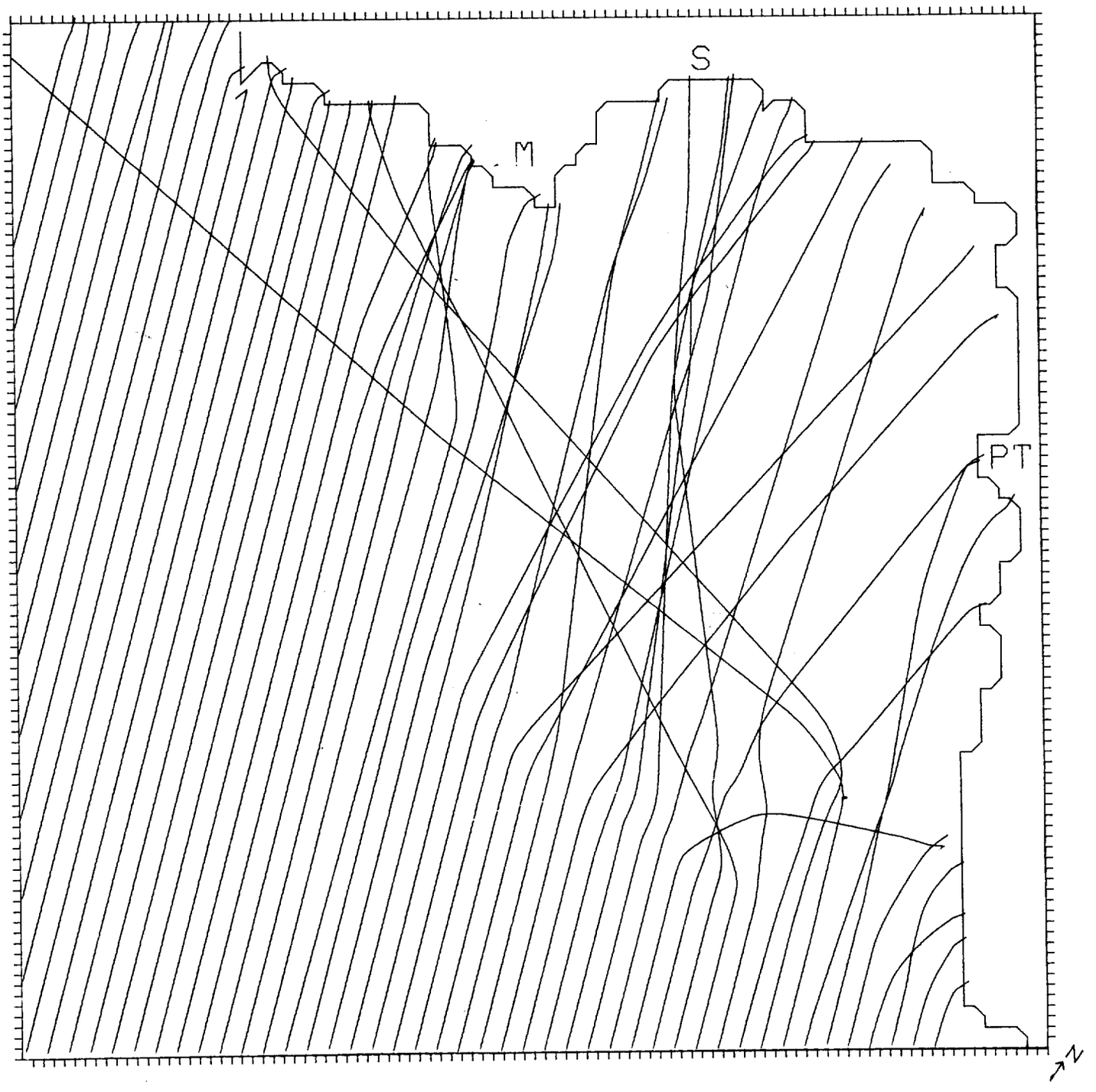

Figure C15